Coherent -electron dynamics of (P)-2,2-biphenol induced by ultrashort linearly polarized UV pulses: Angular momentum and ring current

H. Mineo, S. H. Lin, and Y. Fujimura

Citation: The Journal of Chemical Physics **138**, 074304 (2013); doi: 10.1063/1.4790595
View online: http://dx.doi.org/10.1063/1.4790595
View Table of Contents: http://scitation.aip.org/content/aip/journal/jcp/138/7?ver=pdfcov
Published by the AIP Publishing

Coherent π-electron dynamics of (*P*)-2,2′-biphenol induced by ultrashort linearly polarized UV pulses: Angular momentum and ring current

H. Mineo,[1] S. H. Lin,[1,2] and Y. Fujimura[1,3,a)]
[1]*Institute of Atomic and Molecular Sciences, Academia Sinica, Taipei 10617, Taiwan*
[2]*Department of Applied Chemistry, Institute of Molecular Science and Center for Interdisciplinary Molecular Science, National Chiao-Tung University, Hsin-Chu 300, Taiwan*
[3]*Department of Chemistry, Graduate School of Science, Tohoku University, Sendai 980-8578, Japan*

(Received 8 November 2012; accepted 22 January 2013; published online 15 February 2013)

The results of a theoretical investigation of coherent π-electron dynamics for nonplanar (*P*)-2,2′-biphenol induced by ultrashort linearly polarized UV pulses are presented. Expressions for the time-dependent coherent angular momentum and ring current are derived by using the density matrix method. The time dependence of these coherences is determined by the off-diagonal density matrix element, which can be obtained by solving the coupled equations of motion of the electronic-state density matrix. Dephasing effects on coherent angular momentum and ring current are taken into account within the Markov approximation. The magnitudes of the electronic angular momentum and current are expressed as the sum of expectation values of the corresponding operators in the two phenol rings (*L* and *R* rings). Here, *L* (*R*) denotes the phenol ring in the left (right)-hand side of (*P*)-2,2′-biphenol. We define the bond current between the nearest neighbor carbon atoms C_i and C_j as an electric current through a half plane perpendicular to the C_i–C_j bond. The bond current can be expressed in terms of the inter-atomic bond current. The inter-atomic bond current (bond current) depends on the position of the half plane on the bond and has the maximum value at the center. The coherent ring current in each ring is defined by averaging over the bond currents. Since (*P*)-2,2′-biphenol is nonplanar, the resultant angular momentum is not one-dimensional. Simulations of the time-dependent coherent angular momentum and ring current of (*P*)-2,2′-biphenol excited by ultrashort linearly polarized UV pulses are carried out using the molecular parameters obtained by the time-dependent density functional theory (TD-DFT) method. Oscillatory behaviors in the time-dependent angular momentum (ring current), which can be called angular momentum (ring current) quantum beats, are classified by the symmetry of the coherent state, symmetric or antisymmetric. The bond current of the bridge bond linking the *L* and *R* rings is zero for the symmetric coherent state, while it is nonzero for the antisymmetric coherent state. The magnitudes of ring current and ring current-induced magnetic field are also evaluated, and their possibility as a control parameter in ultrafast switching devices is discussed. The present results give a detailed description of the theoretical treatment reported in our previous paper [H. Mineo, M. Yamaki, Y. Teranish, M. Hayashi, S. H. Lin, and Y. Fujimura, J. Am. Chem. Soc. **134**, 14279 (2012)]. © *2013 American Institute of Physics*. [http://dx.doi.org/10.1063/1.4790595]

I. INTRODUCTION

Attosecond science and technology have opened up a fascinating research area of electronic dynamics in atoms, molecules, and condensed matters.[1–22] π electrons in aromatic molecules are mobile and highly reactive, and they are subjected to large responses to external electric fields. This means that they have potential usefulness for organic nanoelectronics and optoelectronics.[23,24]

There have been theoretical studies on generation of ring currents or control of π-electron motions in aromatic ring molecules using ultrafast UV pulsed lasers.[25–32] Planar molecules with a single aromatic ring such as Mg porphyrin,[25–27] benzene,[28] and 2,5-dichloro[n](3,6) pyrazinophane[29–32] were target molecules. Mg porphyrin with D_{4h} symmetry and benzene with D_{6h} symmetry can be rotated along each aromatic ring by using circularly polarized UV laser pulses. Here, a degenerate singlet excited state was excited. The direction of π-electron rotations, clockwise or counterclockwise, can be determined by applying right or left circularly polarized laser pulses, and the resultant ring current is unidirectional and decays with a damping constant after the pulse has been switched off. For 2,5-dichloro[n](3,6) pyrazinophane, which is a chiral molecule with planar chirality, a linearly polarized UV laser pulse was used to create π-electron rotations along the ring since the aromatic ring, pyrazine, has no degenerate electronic states.[29] The initial rotational direction is determined by adjusting the photon polarization direction of laser pulses to in-phase or out-of-phase superposition of the quasi-degenerate two excited states: clockwise rotation is induced by in-phase superposition, while counterclockwise rotation is induced by out-of-phase superposition.[29] The angular momentum created is

a)Author to whom correspondence should be addressed. Electronic mail: fujimurayuichi@m.tohoku.ac.jp.

transient and should be referred to as a coherent angular momentum, and the corresponding ring current is also referred to as a coherent ring current. These coherent quantities dephase with a dephasing constant, which mainly originates from an elastic interaction between π electrons and vibrational motions.[31]

Recently, Mineo *et al.*[33] proposed an efficient method for multi-dimensional quantum switching of π-electron rotations in (*P*)-2,2′-biphenol. This is a typical nonplanar chiral aromatic molecule of axial chirality, which has two aromatic rings (called *L* and *R* rings hereafter) linked by the C–C single (bridge) bond. For π electrons in (*P*)-2,2′-biphenol, there are four possible rotational patterns (CC, AA, CA, and AC), where C and A refer to clockwise and anticlockwise rotations, respectively, and the first and second letters in each pattern refer to the left (*L*) and right (*R*) phenol rings, respectively. When a pair of quasi-degenerate π-electronic excited states is coherently excited by ultrashort linearly polarized UV pulses, the generated angular momentum (ring current) on each aromatic ring is also correlated. Because of the nonplanar geometrical structure of (*P*)-2,2′-biphenol, the resultant time-dependent coherent angular momentum is two-dimensional. The directions of these quantities depend on the symmetry of the coherent state and the relative phase of the pair of quasi-degenerate states.

In order to design functioning of organic electronics or optoelectronics, it is essential to quantitatively evaluate magnitudes of angular momentum and ring currents in addition to evaluation of their directions. Many studies on calculations of ring currents in molecules have been performed for interpretation of magnetic properties of conjugated molecular systems.[34,35] Here, systems of interest were with the closed-shell ground state, and current densities were calculated by the first-order perturbation theory. Ring currents of aromatic molecules induced by intense UV laser pulses, on the other hand, are directly concerned with electronic excited states and treatments beyond the first-order perturbation theory are required. In this paper, we present a fundamental theory for quantitative treatment of the coherent electron dynamics of a nonlinear aromatic ring molecule and application of the theory to (*P*)-2,2′-biphenol. In a previous paper,[33] an essential description of quantum switching of electron rotations in (*P*)-2,2′-biphenol was given.

In Sec. II, we derive an expression for coherent π-electron angular momentum and that of the ring current. Equations of motion for π electrons are solved by using the density matrix method. Here, dephasing constants are derived within the Markov approximation.[36–38] An analytical expression for the bond current between two nearest neighboring carbon atoms as well as that of the bridge bond is derived. The ring current in each phenol ring is defined as averaging of the bond currents. In Sec. III, an application of the theory to (*P*)-2,2′-biphenol, which is induced by an ultrashort linearly polarized UV pulse, is presented within a three-excited state model. Quantum beats of coherent angular momentum and ring current of the whole molecule are evaluated as well as those of the two phenol rings using the TD-DFT results. Magnitudes of the coherent ring current-induced magnetic field were calculated to discuss the magnetic property for a control device. The summary and conclusion of this paper are given in Sec. IV.

II. COHERENT π-ELECTRON ANGULAR MOMENTUM AND CURRENT

A. Equations of motion for π electrons in a pulsed laser field

Expectation values of the electric angular momentum and current operators of an aromatic molecule excited by visible or UV light are generally expressed as

$$\langle \hat{O}(\vec{r},t)\rangle = n\int d^3r_1\cdots d^3r_n\delta(\vec{r}-\vec{r}_1)\Psi^*(t)\hat{O}(\vec{r}_1)\Psi(t). \tag{1}$$

Here, $\hat{O}(\vec{r}_1)$ is a one-electron operator for the angular momentum or current, $\Psi(t)$ is an electronic wave function at time *t*, *n* is the number of electrons, and $\vec{r}_i$ denotes the electron coordinates of the *i*th electron. Since we are interested in optically allowed electronic excited states of conjugated aromatic molecules, we expand the electronic wave function in terms of electronic configurations, the ground electronic Φ_0, and singly excited electronic ones Φ_α as

$$\Psi(t) = C_0(t)\Phi_0 + \sum_\alpha C_\alpha(t)\Phi_\alpha, \tag{2}$$

where Φ_0 is given as $\Phi_0(\vec{r}_1,\ldots,\vec{r}_n) = \|\phi_1\cdots\phi_a\cdots\phi_b\cdots\phi_n\|$ with $\phi_n \equiv \phi_n(\vec{r}_n)$. Here, ϕ_a and ϕ_b are among the *n* occupied orbitals, and Φ_α is the electronic wave function for a singly excited electronic configuration α: $a \to a'$, i.e., single electron transition from occupied MO *a* to unoccupied MO *a*′, $\Phi_\alpha(\vec{r}_1,\ldots,\vec{r}_n) = \|\phi_1\cdots\phi_{a'}\cdots\phi_n\|$.

Time-dependent behaviors of electronic dynamics induced by a pulsed laser field, $\vec{E}(t)$, can be directly obtained by solving the coupled equations of motion of the electronic-state density matrix element, $\rho_{\alpha\beta}(t)$, with the initial conditions $\rho_{00}(0) = 1$ and $\rho_{\alpha\alpha}(0) = 0$ for $\alpha \neq 0$;$\rho_{\alpha\beta}(0) = 0$ for $\alpha \neq \beta$,

$$\frac{d\rho_{\alpha\beta}(t)}{dt} = -\frac{i}{\hbar}\sum_\gamma (V_{\alpha\gamma}(t)\rho_{\gamma\beta}(t) - \rho_{\alpha\gamma}(t)V_{\gamma\beta}(t)) - (i\omega_{\alpha\beta} + \gamma_{\alpha\beta})\rho_{\alpha\beta}(t). \tag{3}$$

Here, the density matrix element, $\rho_{\alpha\beta}(t)$, is defined as $\rho_{\alpha\beta}(t) \equiv C_\alpha(t)C^*_\beta(t)$, and $\hat{V}(t)_{\alpha\gamma}$ denotes the coupling between states α and γ through the molecule-field interaction, $\hat{V}(t) = -\vec{\mu}\cdot\vec{E}(t)$, where $\vec{\mu}$ is the transition dipole moment operator, $\omega_{\beta\alpha}$ is the angular frequency difference between two electronic states α and β, and $\gamma_{\alpha\beta}(=\frac{1}{2}(\gamma_\alpha+\gamma_\beta)+\gamma^{(d)}_{\alpha\beta})$ is the dephasing constant in Markov approximation.[39] Here, $\gamma_\alpha(\gamma_\beta)$ is the nonradiative transition rate constant of state α (β), and $\gamma^{(d)}_{\alpha\beta}$ is the pure dephasing constant that is induced by elastic interactions between the molecule of interest and heat baths.

Nonradiative transitions are induced by breakdown of the Born-Oppenheimer approximation in isolated systems.[40,41] Nonradiative transition rate constants depend on vibronic states and their time scales vary from picoseconds to femtoseconds.[42–44] Femtosecond time-resolved pump-probe experiments, such as experiments using femtosecond time-resolved photoelectron imaging spectroscopy,[45] are used to

directly detect ultrafast nonradiative transition rate constants in higher excited states of aromatic molecules. In this paper, the nuclear-frozen approximation was adopted and the magnitudes of dephasing constants adopted are specified in the figure legends.

B. Coherent electric angular momentum

Since we are interested in coherent behaviours of optically active nearly degenerated π-electronic exited states in the visible or UV region of a chiral aromatic ring molecule, we evaluate Eq. (1) in terms of singly excited configurations as

$$\langle \hat{O}(\vec{r}_1, t)\rangle = n \int d^3r_1 \cdots d^3r_n \delta(\vec{r} - \vec{r}_1)(\mathrm{Tr}\rho(t)O(\vec{r}_1)), \quad (4)$$

where $O_{\alpha\beta}(\vec{r}_1) = \langle \Phi_\alpha | \hat{O}(\vec{r}_1) | \Phi_\beta \rangle$. In Eq. (4), the coherence between the ground state and a singly excited state configuration is omitted because the coherence time is short compared with that between singly excited configurations, and only the coherence between singly excited state configurations is taken into account. Our formulation of coherent electric angular momentum is based on treatment within a linear combination of atomic orbitals-molecular orbitals (LCAO MO) approximation.

A π orbital ϕ_k associated with optical transition is expanded in terms of a linear combination of atomic orbitals χ_i as

$$\phi_k = \sum_i c_{k,i}\chi_i, (k = a, a', b, b'), \quad (5)$$

where i specifies the atomic orbital and $c_{k,i}$ is the molecular orbital coefficient.

Equation (4) can be rewritten in terms of Eq. (5) as

$$\langle \hat{O}(\vec{r}, t)\rangle = 2n \sum_{\alpha<\beta} \mathrm{Im}\rho_{\beta\alpha}(t) \sum_{ij} \left(\delta_{ab} c^*_{a'i} c_{b'j} + \delta_{a'b'} c^*_{ai} c_{bj}\right) \times \chi^*_i i \hat{O}(\vec{r}) \chi_j. \quad (6)$$

Here, it should be noted that the time evolution of the expectation value is expressed by the off-diagonal density matrix element. Suffixes (a, a') and (b, b') depend on electronic configurations α and β, respectively.

Let us consider a space-fixed chiral aromatic molecule with two aromatic rings connected with a single bond. The total electron angular momentum operator can be expressed as the sum of the angular momentum operator of each aromatic ring, which is defined as $\hat{O}(\vec{r}) = \vec{l}_{zL} + \vec{l}_{zR}$, where $\vec{l}_{zK} = -i\hbar(x_K \partial / \partial y_K - y_K \partial / \partial x_K)\vec{n}_K$, the electric angular momentum operator of the Z-component of ring K (= L or R). Here, L and R denote the ring on the left-hand side and that on the right-hand side, respectively. Coordinates x_K and y_K are defined on ring K and $\vec{n}_K$ is the unit vector perpendicular to the ring. The expectation value of the angular momentum operator is given, for example, in terms of a $2p_z$ carbon AOs as

$$\langle \vec{l}(t)\rangle = \int d^3r_L \langle \vec{l}_{zL}\rangle + \int d^3r_R \langle \vec{l}_{zR}\rangle \equiv \vec{l}_L(t) + \vec{l}_R(t), \quad (7)$$

where

$$\vec{l}_K(t) \equiv \int d^3r_K \langle \vec{l}_{zK}\rangle = -2n\hbar \vec{n}_K \sum_{\alpha<\beta} \mathrm{Im}\rho_{\beta\alpha}(t) \times \sum_{ij\in K} \left(\delta_{ab} c^*_{a'i} c_{b'j} + \delta_{a'b'} c^*_{ai} c_{bj}\right) \times \frac{x_{K,i} y_{K,j} - x_{K,j} y_{K,i}}{15a_2^2} \left(3 + 3\left(\frac{r_{ij}}{a_2}\right) + \left(\frac{r_{ij}}{a_2}\right)^2\right) \times \exp(-r_{ij}/a_2). \quad (8)$$

Here, a_2 is a constant related to the orbital exponent of the $2p_z$ atomic orbital and r_{ij} is the distance between i and j carbon atom sites. It should be noted in Eq. (8) that the laser intensity dependence in the electron angular momentum is involved in the imaginary part of the off-diagonal density matrices, $\mathrm{Im}\rho_{\beta\alpha}(t)$.

A brief derivation of Eq. (8) is presented in Appendix A.

C. Coherent ring current

An electric current passing through a surface S at time t is generally defined as

$$\langle J(t)\rangle \equiv \int_S d^2r_\perp \vec{n}_\perp \cdot \langle \hat{J}(\vec{r}, t)\rangle. \quad (9)$$

Here, $\vec{n}_\perp$ is a unit vector perpendicular to a surface S and $\langle \hat{J}(\vec{r}, t)\rangle \equiv \langle \Psi(t)|\hat{J}(\vec{r})|\Psi(t)\rangle$.

This can be expressed as

$$\langle \hat{J}(\vec{r}, t)\rangle = 2n \sum_{\alpha<\beta} \mathrm{Im}\rho_{\beta\alpha}(t) \sum_{ij} \left(\delta_{ab} c^*_{a'i} c_{b'j} + \delta_{a'b'} c^*_{ai} c_{bj}\right) \times i\chi^*_i \hat{J}(\vec{r})\chi_j = \frac{2ne\hbar}{m_e} \sum_{\alpha<\beta} \mathrm{Im}\rho_{\beta\alpha}(t) \sum_{ij} \left(\delta_{ab} c^*_{a'i} c_{b'j} + \delta_{a'b'} c^*_{ai} c_{bj}\right) \times \chi^*_i \vec{\nabla} \chi_j, \quad (10)$$

where $\hat{J}(\vec{r}) = \frac{e\hbar}{2m_e i}(\vec{\nabla} - \overleftarrow{\nabla})$ is the current density operator. Here, $\vec{\nabla}(\overleftarrow{\nabla})$ denotes the nabra operating the atomic orbital on the right-hand (left-hand) side. Surface integration in Eq. (9) is carried out over a half-plane S.

Since the L and R rings are not round but consist of nonequivalent C–C bonds, we introduce the bond current $\langle J(t)\rangle_{ij}$ from the nearest neighbor atoms at sites j to i, which is given in terms of inter-atomic bond current (IABC) J_{ij}^{IABC} as

$$\langle J(t)\rangle_{ij} = \frac{2ne\hbar}{m_e} \sum_{\alpha<\beta} \mathrm{Im}\rho_{\beta\alpha}(t) \left(\delta_{ab}\left(c^*_{a'i} c_{b'j} - c^*_{b'i} c_{a'j}\right) + \delta_{a'b'}\left(c^*_{ai} c_{bj} - c^*_{bi} c_{aj}\right)\right) J_{ij}^{\mathrm{IABC}}, \quad (11)$$

where

$$J_{ij}^{\mathrm{IABC}} = \int_S d^2r_\perp \chi^*_i \vec{n}_\perp \cdot \vec{\nabla} \chi_j \left(\equiv J_{ij}^{\mathrm{IABC}(S\ at\ center)}\right). \quad (12)$$

Here, surface S is set to be perpendicular to the C_i and C_j bond at the center, and $\vec{n}_{ij} = \frac{\vec{r}_i - \vec{r}_j}{|\vec{r}_i - \vec{r}_j|}$.

Equation (12) is given in the $2p$ carbon AO basis set, $\{\chi_i\}$, as

$$J_{ij}^{\mathrm{IABC}(S\ at\ center)} = \frac{\cos\theta r_{ij}}{2a_2^6}\int_0^\infty dr \frac{r^3 \exp\left(-2\sqrt{r_{ij}^2/4+r^2}/a_2\right)}{\sqrt{r_{ij}^2/4+r^2}}. \quad (13)$$

Here, $\theta = \pi$ for the bond current of the chemical bond belonging to one of the two aromatic rings, L or R, while $\theta = \theta_d$ for the bridge bond current of bond C_i–C_j with a dihedral angle between the two rings θ_d. C_i (C_j) refers to the bridge carbon belonging to the R (L) ring. A brief derivation of Eq. (13) is shown in Appendix A.

We now define an effective ring current along ring K, $\langle J(t)\rangle_K$, by taking the average over all of the bond currents as

$$\langle J(t)\rangle_K \approx \frac{1}{N_K}\sum_{(ij)\subset K}^{N_K}\langle J(t)\rangle_{ij}, \quad (14)$$

where N_K is the number of bonds of ring K.

III. RESULTS AND DISCUSSION

Figure 1(a) shows the structure of (P)-2,2′-biphenol and the directions of transition dipole moments associated with the electron dynamics of interest. In this paper, (P)-2,2′-biphenol was assumed to be fixed on a surface by a non-conjugated chemical bond or in a space by laser molecular orientation techniques.[46] The laboratory-fixed Y-axis is set to be parallel to the single bond bridging the two phenol groups, and the rotation axis of point group C_2 is placed along the laboratory-fixed Z-axis parallel to the surface normal. The geometry of (P)-2,2′-biphenol in the ground state was optimized by using the DFT B3LYP level of theory in the GAUSSIAN09 program.[47] The 6-31G+(d,p) basis sets were used throughout our calculations. The dihedral angle between the two phenol groups, θ_d, was found to be 108.9° from our DFT calculations.[33] The calculated geometrical structures were given in Ref. 33.

For generation of coherent angular momentum and ring current of (P)-2,2′-biphenol, we focus on the three optically allowed excited states (a, b_1, and b_2) whose energies range from 6.67 to 6.84 eV as shown in Fig. 1(b). The transition energies to the a, b_1, and b_2 states, which were calculated at the optimized ground state geometry using the TD-DFT B3LYP level of theory[33] are 6.67, 6.78, and 6.84 eV, respectively. For comparison, the corresponding transition energies calculated with the *ab initio* CIS/6-31G+(d,p) level of theory were 7.32, 7.35, and 7.45 eV, respectively. Here, the optimized ground state geometry obtained by using the TD-DFT B3LYP level of theory was adopted. The electronic states a, b_1, and b_2 have the same ordering between the TD-DFT and *ab initio* CIS MO methods, although there are considerable deviations in the transition energies.

It is well recognized that TD-DFT is the most widely applied tool for modeling the electronic spectra of organic and inorganic molecules, although TD-DFT poorly estimates

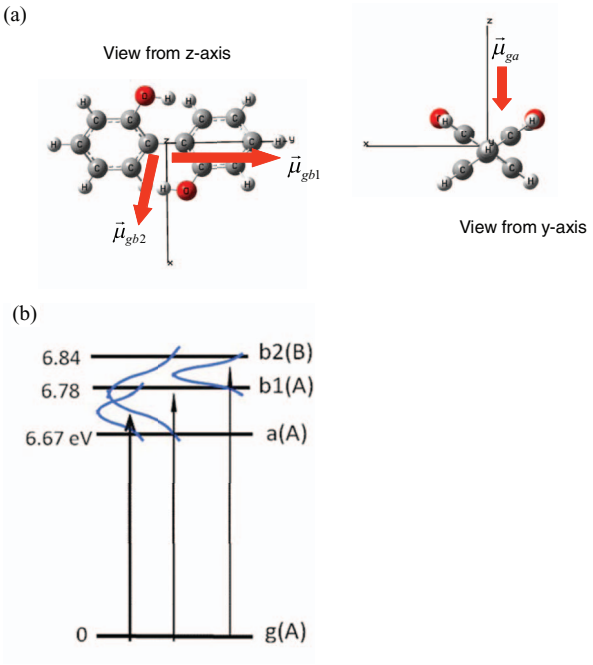

FIG. 1. (a) Geometrical structure of (P)-2,2′-biphenol and transition moment vectors. (b) Three electronic excited states and optical transitions to create the coherent electronic states.

transition frequencies to excited states having a double excited character or a significant charge-transfer nature.[48] For valence transitions, functionals, B3LYP, PBE, and CAM-3LYP provide similar mean absolute deviations.[48] The three optically allowed excited states associated with the present laser-induced electron dynamics have one-electronic excitation configurations since they basically consist of optically allowed $\pi\pi^*$ excited states of two phenol rings. These facts indicate the validity of use of TD-DFT B3LYP level of theory in this paper. Experimental values for energy differences between these two electronic states are directly reflected in the frequencies that appear in the quantum beats in time-resolved photoelectron spectroscopy or coherent angular momentum or ring current proposed in this paper.

The main electronic configuration of state a, Φ_a, is a one-electron excitation configuration from the 46th to 52nd MOs, which is expressed as $\Phi_{46\to52}$. Similarly, those of the two states b_1 and b_2 are expressed as $\Phi_{46\to53}$ and $\Phi_{46\to51}$, respectively. The phase of each MO is schematically shown in Fig. 2. Both the 46th and 52nd MOs belong to the totally symmetric irreducible representation A in the C_2 point group, and $\Phi_{46\to52}$ belongs to A representation. Both $\Phi_{46\to53}$ and $\Phi_{46\to51}$ belong to the antisymmetric irreducible representation B. The transition dipole moment from the ground state to excited state a (A), $\boldsymbol{\mu}_{ga}(= (0, 0, -0.77))$, is parallel to the Z-axis, and the others, $\boldsymbol{\mu}_{gb1}(= (0.08, 1.93, 0))$ and $\boldsymbol{\mu}_{gb2}(= (1.24, -0.34, 0))$, are nearly orthogonal to each other in the XY-plane as shown in Fig. 1(a).[33]

A. Generation of two-state electronic coherence by linearly polarized UV pulses

Preparation of electronic coherence with a definite relative phase between two electronic states, a and b, i.e.,

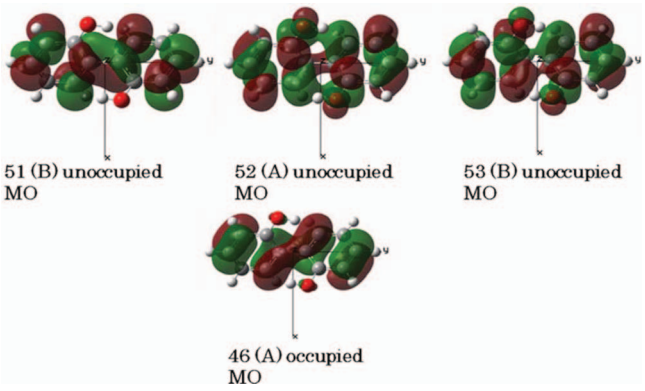

FIG. 2. Occupied and unoccupied MOs relevant to the coherent electronic states. a, b_1, and b_2 electronic states have electronic configurations of $46 \rightarrow 52$, $46 \rightarrow 53$, and $46 \rightarrow 51$, respectively. A (B) denotes the totally symmetric (antisymmetric) irreducible representation of the C_2 point group.

in-phase $(a + b)$ or out-of-phase $(a - b)$, is essential in order to generate coherent angular momentum and electric current in aromatic ring molecules without degenerate electronic states. This is because a coherent state is a nonstationary state expressed in terms of the eigenstates of π-electron angular momentum and therefore a ring current can be transiently created. The method for preparation of electronic coherence by a linearly polarized laser pulse has already been described in Ref. 33.

There exist three types of two-electronic coherent states in the present three-excited state model, which can be represented as $(b_1 + b_2)$ $((b_1 - b_2))$, $(a + b_1)$ $((a - b_1))$, and $(a + b_2)$ $((a - b_2))$. Each electronic coherence at the initial time can be generated by applying a linearly polarized UV laser pulse with a properly selected polarization direction. Because of the nonplanar geometrical structure, the angular momentum is two-dimensional and the ring current is on two different surfaces, depending on the symmetry of the coherent state prepared by the laser pulse: Z-directional angular momentum is generated for the created coherent state with A symmetry and corresponding ring current is generated on the Z-directional angular momentum, while X-directional angular momentum is generated for the coherent state with B symmetry and ring current is generated on the X-directional angular momentum.

A two-state electronic coherence can be generated even in a three-excited state system in which a third excited state is located between the two excited states if two conditions for the applied linearly polarized laser pulse are satisfied. For example, for $(a \pm b_2)$ electronic coherence, the condition for a linearly polarized laser pulse with polarization vector $\vec{e}_\pm$ is given as

$$\vec{\mu}_{ga} \bullet \vec{e}_\pm = \pm \vec{\mu}_{gb2} \bullet \vec{e}_\pm \quad \text{and} \quad \vec{\mu}_{gb1} \bullet \vec{e}_\pm = 0, \tag{15a}$$

or, equivalently,

$$\vec{e}_\pm = \vec{\mu}_{gb1} \times (\vec{\mu}_{gb2} \mp \vec{\mu}_{ga}) / |\vec{\mu}_{gb1} \times (\vec{\mu}_{gb2} \mp \vec{\mu}_{ga})|. \tag{15b}$$

Thus, even laser pulse overlaps with an a, b_1, and b_2, $(a + b_2)$ or $(a - b_2)$ electronic coherent state can be selectively generated. A brief derivation of Eqs. (15) is given in Appendix C.

B. Angular momentum quantum beats

Figure 3 shows time-dependent angular momenta calculated for three types of electronic coherence, $(b_1 + b_2)$, $(a + b_1)$, and $(a + b_2)$, each of which is created by a linearly polarized UVπ-pulse with a properly selected photon polarization direction. The pulse envelope function is shown in the right-hand side of each figure. The pulse amplitude of 0.19 TW/cm^2 is used for $(b_1 + b_2)$ coherence. Those of 0.83 and 3.32 TW/cm^2 are used for $(a + b_1)$ and $(a + b_2)$ coherences, respectively. For $(b_1 + b_2)$ electronic coherence, angular momentum along the Z-axis is generated, while for both $(a + b_1)$ and $(a + b_2)$ electronic coherences, angular momenta along the X-axis are generated with π-phase shift. Similarly, for out-of phase electronic coherences, $(b_1 - b_2)$, $(a - b_1)$, and $(a - b_2)$, each angular momentum can be expressed by that for the corresponding in-phase coherence with π-phase shift. The simple sinusoidal time-dependence originates from creation of two-electronic state coherence, the oscillation period of which corresponds to the frequency difference between the two states. This should be called angular momentum quantum beats, similar to fluorescence quantum beats originating from vibronic coherence in fluorescence.[49] However, it should be noted that in angular momentum quantum beats, π electrons rotate in a unidirectional way a few times within the half cycle of the oscillation. The unidirectional π-electron rotation can produce unidirectional ring current and current-induced magnetic flux. In principle, this makes it possible to design ultrafast switching devices made from organic ring molecules.

The angular momenta, $\vec{l}_Z(t)$ and $\vec{l}_X(t)$, shown in Fig. 3 are calculated from the summation of the electric angular momenta generated in the two aromatic rings $\vec{l}_L(t)$ and $\vec{l}_R(t)$ by using the relation $\vec{l}_Z(t) = 2\vec{l}_L(t) \sin \frac{\theta_d}{2}$ with $\vec{l}_L(t) = \vec{l}_R(t)$ and $\vec{l}_X(t) = 2\vec{l}_L(t) \cos \frac{\theta_d}{2}$ with $\vec{l}_L(t) = -\vec{l}_R(t)$. Here, dephasing constants, $\gamma_{ab_1} = \gamma_{ab_2} = \gamma_{b_1b_2} = 0.01$ eV, were adopted. Table I shows these angular momenta of (P)-2,2′-biphenol with $\theta_d = 108.9^\circ$ at the maximum electronic coherence time, $t = t^*$, i.e., the magnitude of the imaginary part of the corresponding density matrix element has the maximum, $\mathrm{Im}\rho_{\alpha\beta}(t^*) = -\frac{1}{2}$. Here, dephasing effects were omitted. This results in $\vec{l}_X(t^*) > 0$ or $\vec{l}_X(t^*) < 0$ for the $(a + b_1)$ and $(a + b_2)$ electronic coherences and in $\vec{l}_Z(t^*) < 0$ for the $(b_1 + b_2)$ electronic coherence.

TABLE I. Angular momenta of the two phenol rings, l_L and l_R, and the resultant angular momenta l_X an l_Z at the maximum coherence.[a]

	$l/\hbar$			
Electronic coherence	l_L	l_R	l_X	l_Y
$(a + b_1)$	− 1.09	1.09	− 1.27	0
$(a + b_2)$	0.17	− 0.17	0.20	0
$(b_1 + b_2)$	− 1.44	− 1.44	0	− 2.34

[a]Maximum coherence is given at $\mathrm{Im}\rho_{b2,b1} = \mathrm{Im}\rho_{b1,a} = \mathrm{Im}\rho_{b2,a} = -1/2$. $l_X = 2l_L \cos \frac{\theta_d}{2} = 1.163l_L = -1.163l_R$ for $(a + b_1)$ or $(a + b_2)$ electronic coherence; $l_Z = 2l_L \sin \frac{\theta_d}{2} = 1.627l_L = 1.627l_R$ for $(b_1 + b_2)$ electronic coherence with dihedral angle $\theta_d(=108.9^\circ)$ between the two phenol rings.

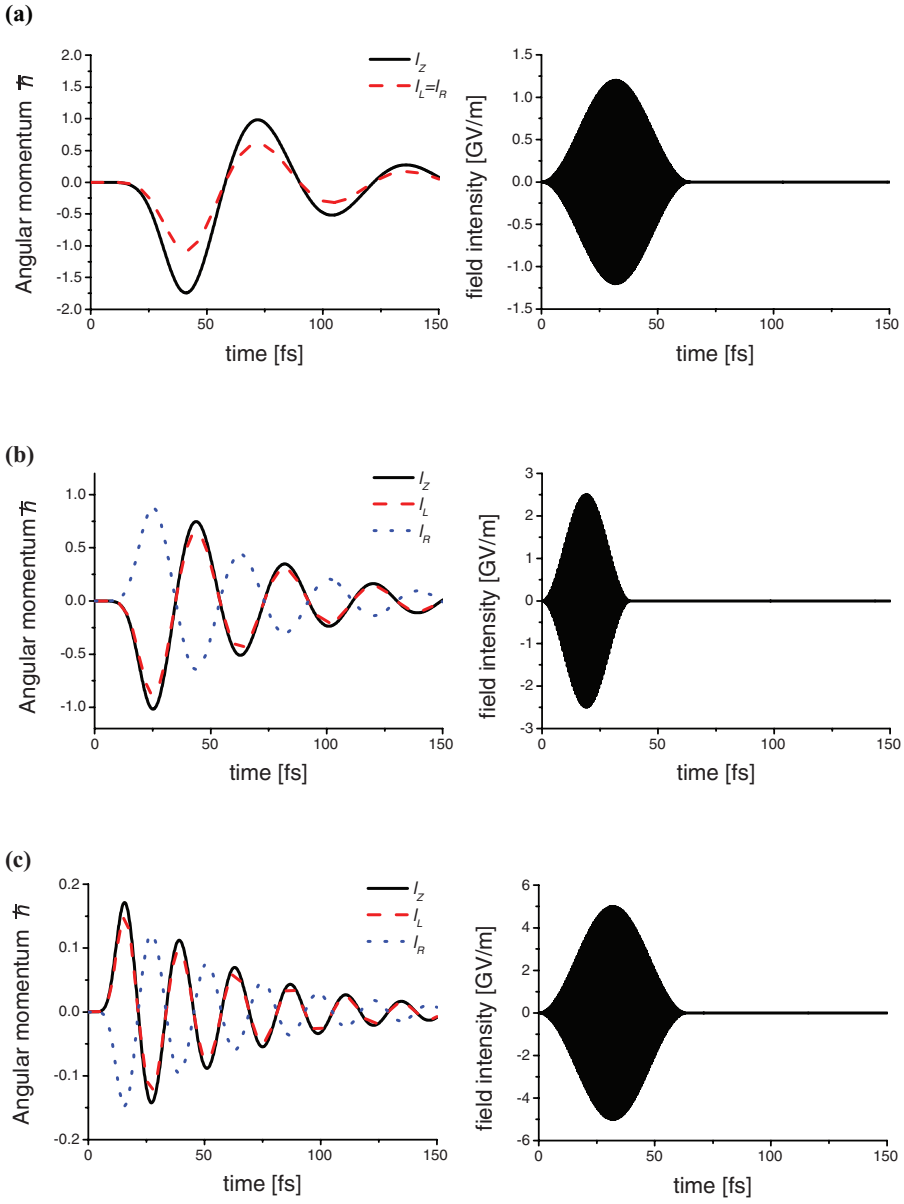

FIG. 3. Time evolution of coherent angular momentum (left-hand side) created by π pulse excitation (right-hand side): (a) for $(b_1 + b_2)$ electronic coherence created by pulse with the amplitude of 0.19 TW/cm^2, (b) for $(a + b_1)$ electronic coherence created by pulse with the amplitude of 0.83 TW/cm^2, and (c) for $(a + b_2)$ electronic coherence created by pulse with the amplitude of 3.32 TW/cm^2. Dephasing constants were set as $\gamma_{b1b2} = \gamma_{ab1} = \gamma_{ab2} = 0.01$ eV (1/50 fs^{-1}).

C. Bond currents and time evolution of coherent ring current

The magnitudes of bond current, J_{ij}, which is calculated at the maximum coherence time, are summarized in Fig. 4 together with the initial direction of the bond currents for three types of electronic coherence. The arrow along each bond of (*P*)-2,2′-biphenol in Fig. 4 denotes the initial direction of the bond current. Magnitudes of the averaged ring current at the maximum coherence time are an order of tens of μA, that is, $\bar{J} = 161$, 86.5, and 63.4 μA for $(b_1 + b_2)$, $(a + b_1)$, and $(a + b_2)$ coherences, respectively.

If the phenol ring is assumed to be a ring with radius r and magnitude of the angular momentum $l = rp$ with linear momentum of electron, p, is given, the ring current J can be estimated by using the relation $2\pi r J = \frac{ep}{m_e}$. Ring currents of 216, 163.5, and 25.5 μA are obtained for the $(b_1 + b_2)$, $(a + b_1)$, and $(a + b_2)$ coherences, respectively. The magnitude of each ring current is large compared with that of the corresponding averaged one. The difference in the magnitudes between the two cases mainly originates from the fact that phenol ring has a functional OH group.

Barth *et al.* reported an electronic current of 84.5 μA for Mg-porphyrin by applying a circularly polarized UV intense laser pulse to yield population inversion.[26] It is interesting that (*P*)-2,2′-biphenol and Mg-porphyrin have the same order of ring current values, though they have different numbers of electrons and different radii of their rotation.

(a) ($b_1 + b_2$) electronic coherence

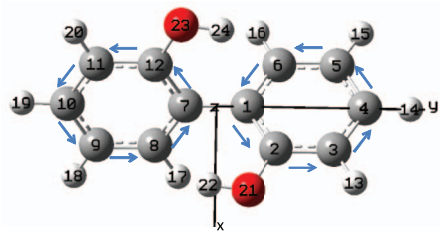

$$|J_{1,2}| = |J_{12,7}| = 181,\ |J_{4,5}| = |J_{9,10}| = 177$$
$$|J_{2,3}| = |J_{11,12}| = 171,\ |J_{5,6}| = |J_{8,9}| = 140$$
$$|J_{3,4}| = |J_{10,11}| = 143,\ |J_{6,1}| = |J_{7,8}| = 156$$
$$|J_{1,7}| = 0,\ |\bar{J}| = 161\ [\mu\text{A}]$$

(b) (a+b_1) electronic coherence

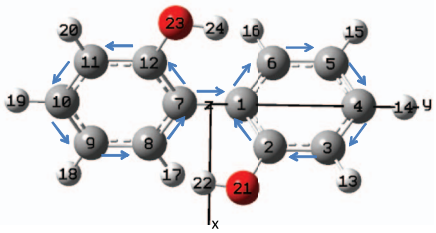

$$|J_{1,2}| = |J_{12,7}| = 101,\ |J_{4,5}| = |J_{9,10}| = 63.2$$
$$|J_{2,3}| = |J_{11,12}| = 86.0,\ |J_{5,6}| = |J_{8,9}| = 85.0$$
$$|J_{3,4}| = |J_{10,11}| = 68.9,\ |J_{6,1}| = |J_{7,8}| = 115$$
$$|J_{1,7}| = 52.3,\ |\bar{J}| = 86.5\ [\mu\text{A}]$$

(c) ($a + b_2$) electronic coherence

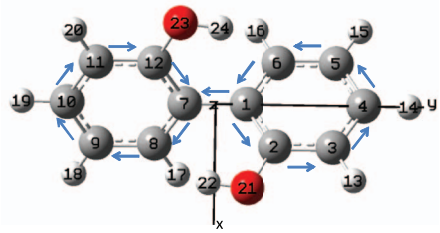

$$|J_{1,2}| = |J_{12,7}| = 64.8,\ |J_{4,5}| = |J_{9,10}| = 39.1$$
$$|J_{2,3}| = |J_{11,12}| = 61.9,\ |J_{5,6}| = |J_{8,9}| = 48.0$$
$$|J_{3,4}| = |J_{10,11}| = 79.2,\ |J_{6,1}| = |J_{7,8}| = 87.5$$
$$|J_{1,7}| = 7.4,\ |\bar{J}| = 63.4\ [\mu\text{A}]$$

FIG. 4. Bond currents J_{ij} for the three types of electronic coherence at $t = t^*$ when the maximum coherence is created, i.e., $\text{Im}\rho_{b2,b1}(t^*) = -1/2$, $\text{Im}\rho_{b1,a}(t^*) = -1/2$, or $\text{Im}\rho_{b2,a}(t^*) = -1/2$. $\bar{J}$ denotes the averaged ring current given by Eq. (14). The blue arrows above C–C bonds denote the initial direction of the currents. Dephasing effects were omitted. Note that the bridge current $J_{1,7} = 0$ for $(b_1 + b_2)$ electronic coherence, while $J_{1,7} \neq 0$ for the other two $(a + b_1)$ and $(a + b_2)$ electronic coherences. The same magnitudes of pulses as those in Fig. 3 were used.

It should be noted that the definition of ring current depends on the choice of half-plane S in the present treatment. For an extreme choice, the half plane is set at each carbon nuclei of the aromatic rings. For such S, the inter-

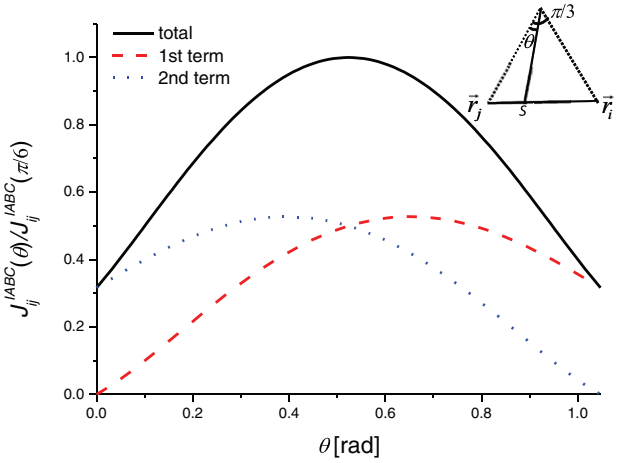

FIG. 5. Inter-atomic bond current $J_{ij}^{\text{IABC}}(\theta)$ as a function of θ. The values are normalized by $J_{ij}^{\text{IABC}}(\pi/6)(= J_{ij}^{\text{IABC}(S\ at\ center)})$. θ, $(0 \le \theta \le \pi/3)$ is defined in the inserted figure. Here, r_i and r_j are the positions of two atomic sites of the bond. s is the position of the half plane S. $J_{ij}^{\text{IABC}}(\theta) = \frac{1}{2}\int_S d^2r_\perp \vec{n}_\perp \cdot \chi_i^* \vec{\nabla} \chi_j - \frac{1}{2}\int_S d^2r_\perp \vec{n}_\perp \cdot \chi_i^* \overleftarrow{\nabla} \chi_j$. The red broken line refers to the first term of $J_{ij}^{\text{IABC}}(\theta)$ and the blue dotted line refers to the second term. The black line indicates the total value of $J_{ij}^{\text{IABC}}(\theta)$.

atomic bond current calculated by using Eq. (12) can be approximately expressed in the $2p$ carbon AO basis set as $J_{ij}^{\text{IABC}(S\text{ at site})} = 0.32 J_{ij}^{\text{IABC}(S\text{ at center})}$ (see Appendix B). Here, $J_{ij}^{\text{IABC}(S\text{ at center})}$ and $J_{ij}^{\text{IABC}(S\text{ at site})}$ denote the inter-atomic bond current obtained by integration over the half plane of surface S perpendicular to the chemical bond at the center and that at the carbon bond site, respectively. A general case of the inter-atomic bond current in which S is set at a position between bond C_i–C_j is considered in Appendix B as well. Figure 5 shows the inter-atomic bond current $J_{ij}^{\text{IABC}}(\theta)$ as a function of θ. The values of $J_{ij}^{\text{IABC}}(\theta)$ are normalized by $J_{ij}^{\text{IABC}}(\pi/6)(= J_{ij}^{\text{IABC}(S\text{ at center})})$. Angle θ $(0 \le \theta \le \pi/3)$ is defined in the inserted figure. $2p_z$ Slater AOs are used. In Fig. 5, $J_{ij}^{\text{IABC}}(\theta) = \frac{1}{2}\int_S d^2r_\perp \vec{n}_\perp \cdot \chi_i^* \vec{\nabla} \chi_j - \frac{1}{2}\int_S d^2r_\perp \vec{n}_\perp \cdot \chi_i^* \overleftarrow{\nabla} \chi_j$ is plotted. The values of the first (second) term of $J_{ij}^{\text{IABC}}(\theta)$ is indicated in a red broken (blue dotted) line. The values of $J_{ij}^{\text{IABC}}(\theta)$ are plotted by the black line. It can be seen from Fig. 5 that the ring current calculated on S perpendicular to bond C_i–C_j at the center has the maximum magnitude, while that on S at carbon nuclei has the minimum magnitude. The averaged value of the current is given as $\frac{1}{\pi/3}\int_0^{\pi/3} d\theta\, J_{ij}^{\text{IABC}}(\theta) = 0.742 J_{ij}^{\text{IABC}(S\text{ at center})}$. This indicates that the magnitudes of the inter-atomic bond current calculated at the center are approximately overestimated by 25%.

Figure 6 shows the time evolution of the ring currents, $J_R(t)$ and $J_L(t)$, which are averaged over the bond currents of the R and L rings, respectively, and that of the bridge bond current, $J_B(t)$. In Fig. 6(a), for the $(b_1 + b_2)$ electronic coherence, $J_R(t)$ and $J_L(t)$ oscillate with the same phase and $J_B(t)$ vanishes. The resultant coherent ring current is generated clockwise or anticlockwise. Effects of dephasing constant are also shown in Fig. 6(a). Here, two cases with $\gamma_{\text{b1b2}} = 0.01$ eV

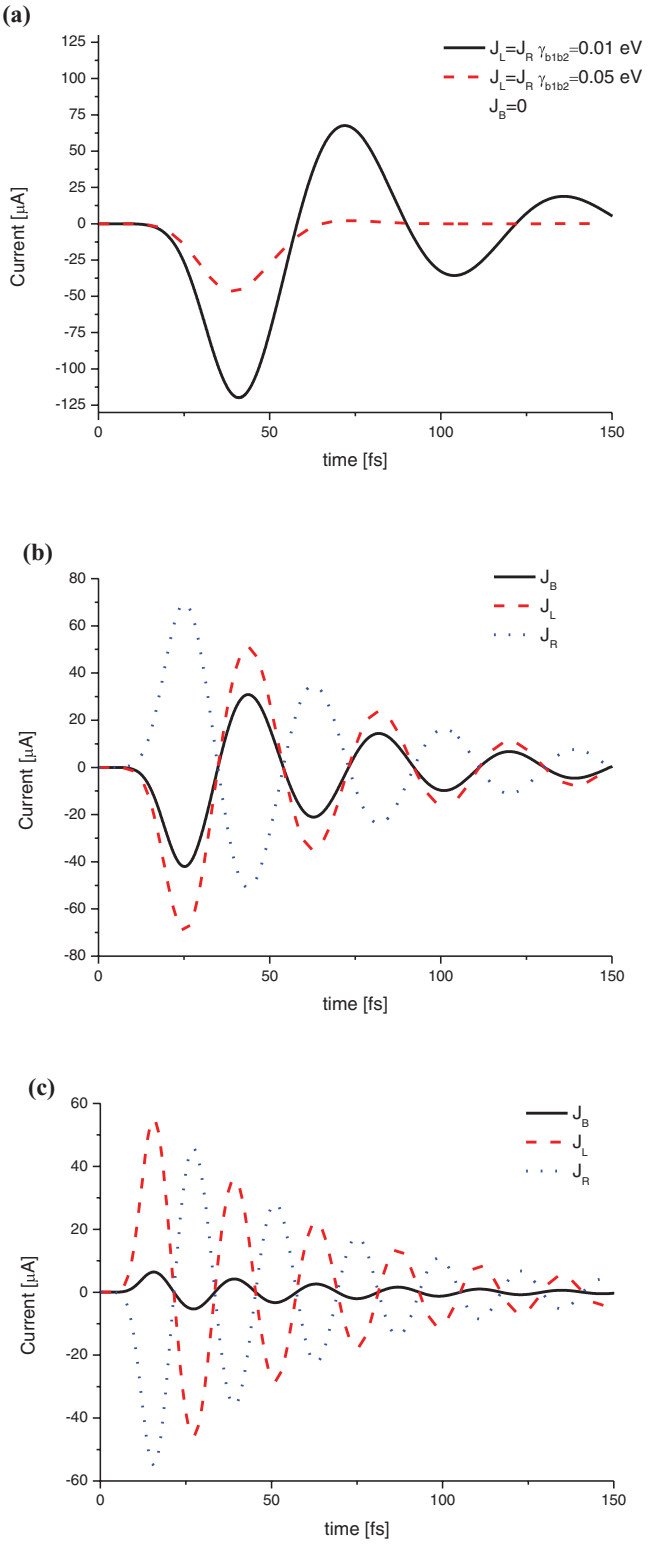

FIG. 6. Time evolution of coherent ring currents created by a π pulse excitation. J_R and J_L denote the ring currents created on R and L rings, respectively. The same pulse excitation conditions as those shown in Fig. 3 are used. J_B denotes the ring current created on the bridging bond: (a) for $(b_1 + b_2)$ electronic coherence, (b) for $(a + b_1)$ electronic coherence, and (c) for $(a + b_2)$ electronic coherence. Dephasing constants were set as $\gamma_{b1b2} = 0.01$ eV (1/50 fs^{-1}) and 0.05 eV (1/10 fs^{-1}) for (a); $\gamma_{ab1} = \gamma_{ab2} = 0.01$ eV for (b) and (c). The same magnitudes of pulses as those in Fig. 3 were used.

(1/50 fs^{-1}) and 0.05 eV (1/10 fs^{-1}) are considered. The black line refers to $J_R(t)$ ($J_L(t)$) calculated with $\gamma_{b1b2} = 0.01$ eV, while the red broken line refers to that $\gamma_{b1b2} = 0.05$ eV (1/10 fs^{-1}). The latter corresponds to the case in which the dephasing width covers the two excited states, b_1 and b_2. In this case, coherent current appears only during the initial half cycle of oscillations as shown in Fig. 6(a). This indicates that the information on the initial phase of coherent ring current, which depends on the polarization direction of an applied linearly polarized pulse,[29,33] may be observed even under such ultrafast dephasing conditions. For the other two cases (b) and (c), $\gamma_{ab1} = \gamma_{ab2} = 0.01$ eV are adopted. For a coherent excitation of a and b_1 states, as shown in Fig. 6(b), $J_R(t)$ and $J_L(t)$ oscillate with opposite phases. The characteristic feature is that nonzero $J_B(t)$ is generated. This feature can also be seen for $(a + b_2)$ electronic coherence shown in Fig. 6(c). $J_B(t)$ oscillates with the same phase as that of $J_R(t)$ for both $(a + b_1)$ and $(a + b_2)$ coherences.

It should be noted that there is a difference between the mechanism of a unidirectional π-electron ring current in aromatic molecules with degenerated electronic states, Mg-porphyrin[25–27] and benzene,[28] and that of a coherent π-electron ring current in a nondegenerate aromatic molecule, (*P*)-2,2′-biphenol.[33] For the former molecules, selective excitation from the ground to one of the degenerated electronic excited states by a left or right circularly polarized UV laser pulse is the mechanism, i.e., incoherent excitation, while for (*P*)-2,2′-biphenol, creation of coherence of two nondegenerate electronic excited states by an ultrashort linearly polarized pulse is the mechanism. For example, Nobusada and Yabana[28] have shown by first-order perturbation treatment that the magnitude of a ring current for benzene is proportional to the square of the electric field of the circularly polarized laser pulse. Under intense circularly polarized laser pulse field conditions, Barth and Manz[26] carried out a quantum model simulation of periodic electron circulation for Mg porphyrin in a target degenerate electronic excited state (Φ_α) with $\alpha = +$ or $-$. In the electronic wavepacket treatment, the state at time t, $\Psi(t)$ is given as

$$\Psi(t) = C_0(t)\Phi_0 + C_\alpha(t)\exp\left[-i\Delta\omega_{\alpha 0}t - \frac{\gamma_\alpha t}{2}\right]\Phi_\alpha. \quad (16)$$

Here, $C_\alpha(t)$ is the coefficient of Φ_α, and $\Delta\omega_{\alpha 0}$ is the frequency difference between the excited state and the ground state. The electric current is simply given as $\langle J(t)\rangle \equiv \int_S d^2r_\perp \vec{n}_\perp \cdot \langle \hat{J}(\vec{r}, t)\rangle$. Here, current density $\langle \hat{J}(\vec{r}, t)\rangle$ is expressed in the LCAOMO approximation (see Sec. II B) as

$$\langle \hat{J}(\vec{r}, t)\rangle = n|C_\alpha(t)|^2 \exp[-\gamma_\alpha t] \times \sum_{ij}\left(\delta_{ab}c^*_{a'i}c_{b'j} + \delta_{a'b'}c^*_{ai}c_{bj}\right)\chi^*_i \hat{O}(\vec{r})\chi_j. \quad (17)$$

This indicates that the current density is proportional to the population of the degenerate electronic excited state and decays exponentially due to population decay after an ultrashort pulse excitation. Effects of pulse excitations are included in $C_\alpha(t)$.

D. Coherent ring current-induced magnetic field

We now evaluate the magnetic field induced by a coherent ring current since magnetic flux is a control parameter for switching devices as well as the ring current.[50–52] There have been several reports on calculations of magnetic fields of molecules in intense laser pulses.[53–55] The magnetic flux density along the central axis perpendicular to ring K (=L or R) is given in a simple ring loop (SRL) model as

$$B_K(t, h) = \frac{\mu_0 \langle J(t) \rangle_K}{2r} \sin^3 \eta. \quad (18)$$

Here, $\mu_0 = 4\pi 10^{-7}$ $W_b A^{-1} m^{-1}$ is the vacuum magnetic permittivity, r $(=r_{ij})$ is the radius of the ring, and $\eta (= \sin^{-1}(r/\sqrt{r^2+h^2}))$ is the angle between the Z-axis and a straight line drawn from the point on ring K, that crosses the Z-axis. $B_K(t, 0)$ at $\eta = \pi/2$ is the value measured at the center of ring K. For $(b_1 + b_2)$ coherent excitation, as shown in Fig. 4(a), the magnitude of $B_K(t, 0)$ at the center of the ring with $r = 0.14$ nm for $\langle J(t) \rangle_K = 100$ μA is 448 mT. The value of $B_K(t, 0)$ oscillates with the same phase of $\langle J(t) \rangle_K$. It is necessary to check that the value is larger than the value corresponding to magnetic field B_{Laser} induced by the intense laser field E applied when we are interested in the induced magnetic fields at an early time regime of an ultrashort excitation laser pulse. The magnitude of B_{Laser} can be obtained by $|B_{\text{Laser}}| = |E|/c$ with $c = 3.0 \times 10^8$ ms^{-1}.The calculated magnitude of B_{Laser} with $|E| = 1.0$ GV/m was about 7.5 $B_K(t, 0)$, which is the same order as that induced by ring current $J = 100$ μA. This means that careful examination is necessary to measure current-induced magnetic flux and to use the magnetic device as a control tool during the pulse duration. In other words, the current-induced magnetic field after the laser pulse is over can be used as a control parameter. Furthermore, quasi-degenerate electronic states with a slow dephasing time constant should be selected to observe the coherent ring current-induced magnetic field.

To prove the coherent ring current-induced magnetic field in the SRL model, Fig. 7 shows the behaviors of the ring current-induced magnetic fields for the $(b_1 + b_2)$ electronic coherence as a function of height h above the Z-axis at $t = t^*$ under the maximum coherence condition, $\text{Im}\rho_{\alpha\beta}(t^*) = -1/2$. The black curve denotes the h-dependence of the coherent ring current-induced magnetic field in the SRL model, $B_K^{\text{SRL}}(t^*, h)$. For checking the validity of the SRL model, the induced magnetic fields calculated with the coherent ring current density, $B_K(t^*, h)$, which is beyond the SRL model, are shown as a function of h (red curve in Fig. 7). The derivation of $B_K(t, h)$ is briefly presented in Appendix D. It can be seen from Fig. 7 that the magnitudes of $B_K^{\text{SRL}}(t^*, h)$ are overestimated near the plane of the aromatic ring $0 \le h < 1$ Å and that the magnitudes are valid for $h > 1$ Å. At the center of the aromatic-ring plane, we have $B_K(t^*, h = 0) = 0.66 B_K^{\text{SRL}}(t^*, h = 0)$, which was evaluated by using the $2p_z$ Slater AOs. The behavior of $B_K^{\text{SRL}}(t^*, h)$ can be explained by the fact that the current density of π electrons is densely distributed over the aromatic ring. We note that a subtle deviation between $B_K^{\text{SRL}}(t^*, h)$ and $B_K(t^*, h)$ in the large h, though $B_K^{\text{SRL}}(t^*, h \to \infty) = 0$ and $B_K(t^*, h \to \infty) = 0$ go to zero.

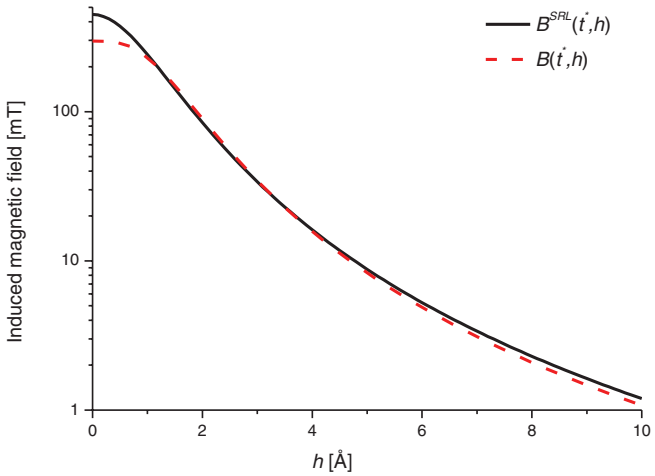

FIG. 7. Induced magnetic fields for the $(b_1 + b_2)$ electronic coherence as a function of height h from the center of aromatic ring K at the time of maximum coherence $t = t^*$. $B_K^{\text{SRL}}(t^*, h)$ and $B_K(t^*, h)$ are the induced magnetic field calculated by a SRL model and that calculated by a distribution of the current density, respectively.

This originates from the fact that aromatic ring is not a perfect ring.

So far, we have considered a ring current-induced magnetic field of chiral aromatic molecules, in which a pair of two nondegenerate electronic excited states is coherently excited by intense linearly polarized UV pulses. We now briefly discuss a ring current-induced magnetic field for *degenerate* electronic excited states of an aromatic molecule induced by an intense *circularly polarized* UV pulse. Yuan and Bandrauk[2] have shown by numerical simulations that circularly polarized attosecond pulses are generated from molecular high-order harmonic generation by ultrashort intense bichromatic circularly and linearly polarized laser pulses. This provides the possibility for circularly polarized attosecond ultraviolet pulses to generate a ring current-induced magnetic field in highly symmetric aromatic molecules. The ring current-induced magnetic field $B(t, h)$ can be calculated on the basis of wave packet treatment as shown in Sec. III C. In the SRL model, we have $B^{\text{SRL}}(t, h) = \frac{\mu_0 J(t)}{2r} \sin^3 \eta$. Here, $J(t)$ is the electric current of the degenerated electronic state of interest. Let us now estimate the magnitude of ring current-induced magnetic field of benzene, which is a typical example of high symmetric aromatic molecules. The electronic spectrum is characterized by the optical allowed transition to the third singlet electronic excited state ($^1E_{1u}$) from the ground state. For the equal population between the two states at $t = t^*$, $B^{\text{SRL}}(t^*, 0) = 874$ mT was obtained using $J(t^*) = 195$ μA that was evaluated within the π electron approximation.[56]

E. Bridge bond current density

From the symmetry consideration of (*P*)-2,2′-biphenol belonging to the C_2 point group, the value of the bridge bond current for $(b_1 + b_2)$ or $(b_1 - b_2)$ electronic coherence vanishes, while that for $(a + b_1)$ $((a - b_1))$ or $(a + b_2)$ $((a - b_2))$

does not vanish. In fact, the bridge bond current density can be calculated in terms of the $2p_z$ orbital of the carbon at the site of each ring, R and L, as

$$\chi_R^* \vec{\nabla} \chi_L = \frac{\exp(-|\vec{r}-\vec{r}_L|/a_2 - |\vec{r}-\vec{r}_R|/a_2)}{\pi a_2^5} \vec{n}_R \cdot \vec{r} \left(\vec{n}_L - \vec{n}_L \cdot (\vec{r}-\vec{r}_L) \frac{\vec{r}-\vec{r}_L}{a_2 |\vec{r}-\vec{r}_L|} \right), \quad (19)$$

where $\chi_K = \frac{\vec{n}_K \cdot (\vec{r}-\vec{r}_K)}{\sqrt{\pi a_2^5}} \exp(-|\vec{r}-\vec{r}_K|/a_2)$ for the $2p_z$ orbital of the carbon at bridge site K ($=L$ or R), $\vec{n}_L = (\cos\frac{\theta_d}{2}, 0, \sin\frac{\theta_d}{2})$, $\vec{n}_R = (-\cos\frac{\theta_d}{2}, 0, \sin\frac{\theta_d}{2})$, and $\vec{r}_R = (0, r_{ij}/2, 0) = -\vec{r}_L$. Here, r_{ij} denotes the bridge bond length.

The values of bridge bond current density along the X-,Y-, and Z-directions on YZ-, ZX-, and XY- planes are, respectively, given by

$$\vec{n}_x \cdot \chi_R^* \vec{\nabla} \chi_L \big|_{x=0} = z \frac{\exp\left(-\sqrt{(y+r_{ij}/2)^2+z^2}/a_2 - \sqrt{(y-r_{ij}/2)^2+z^2}/a_2\right) \sin\theta_d}{2\pi a_2^5}, \quad (20a)$$

$$\vec{n}_y \cdot \chi_R^* \vec{\nabla} \chi_L \big|_{y=0} = \frac{r_{ij} \exp\left(-\frac{2}{a_2}\sqrt{x^2+z^2+r_{ij}^2/4}\right)}{2\pi a_2^6 \sqrt{x^2+z^2+r_{ij}^2/4}} \left(x^2 \cos^2\frac{\theta_d}{2} - z^2 \sin^2\frac{\theta_d}{2} \right), \quad (20b)$$

and

$$\vec{n}_z \cdot \chi_R^* \vec{\nabla} \chi_L \big|_{z=0} = -x \frac{\exp\left(-\sqrt{(y+r_{ij}/2)^2+x^2}/a_2 - \sqrt{(y-r_{ij}/2)^2+x^2}/a_2\right) \sin\theta_d}{2\pi a_2^5}. \quad (20c)$$

In Fig. 8, the bridge bond current density calculated at the maximum coherence is drawn for the $(a + b_1)$ electronic coherence. The direction of the current density flow is perpendicular to the ZX-plane and flows along the Y-axis. The area denoted by positive current indicates that the current flows from the back (L ring) to the front (R ring), while the area denoted by negative current indicates the reverse current flow. The bridge bond current is defined as the integration of all of the areas shown in Fig. 8. The resultant bridge bond current of (P)-2,2′-biphenol has a positive value, which means the current flows in the positive direction along the Y-axis as shown in Fig. 4. Note that the phase of $J_B(t)$ for $(a + b_1)$ is the same as that for $J_L(t)$ as shown in Fig. 4. This can be verified by calculation of the bridge bond current as shown in Fig. 8.

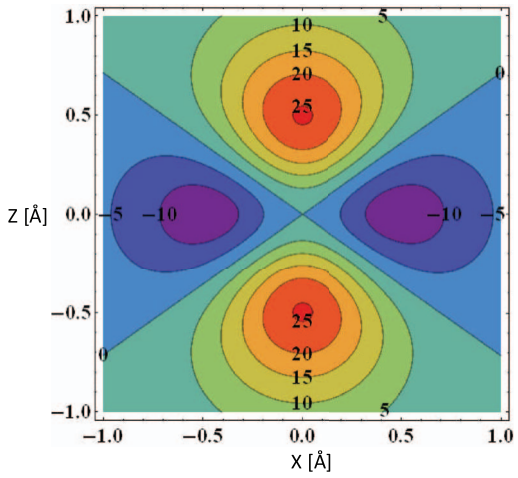

FIG. 8. Contour plot of the bridge bond current density [μA/ Å^2] on the perpendicular plane at the bond center, which is calculated at the maximum value for the $(a + b_1)$ electronic coherence at $t = t^*$. The region in which the current density flows from the back (L ring) to the front (R ring) is denoted by positive values, while the region in which the current density flows from the front to the back is denoted by negative values.

IV. SUMMARY AND CONCLUSION

In this paper, we presented the results of a theoretical study on coherent quantum dynamics of π electrons in (P)-2,2′-biphenol. (P)-2,2′-biphenol is a typical nonplanar chiral aromatic molecule with axial chirality, and a pair of quasi-degenerate excited states in the two phenol rings is coherently excited by an ultrashort linearly polarized UV pulse. This results in the generation of coherent two-dimensional angular momentum and resultant ring current on two different molecular planes. An expression for the coherent π-electron angular momentum and that for the ring current are derived by the density matrix method within the Markov approximation. In a previous study, these expressions were used to investigate quantum switching of π electrons by applying linearly polarized UV laser pulses.[33] A coherent ring current along each phenol ring is defined as the average of bond currents. The bond current is given as the electric current through a half plane S perpendicular to the bond at the center, and the expression for bond current is derived within a LCAO MO approximation. Magnitudes of the electric current defined depend on the position of S on the bond. The position-dependence of the electric current was discussed. The electric current through S at the center of the bond gives the maximum magnitude, while for an ex-

treme case in which S is defined at the bond site, the electric current gives the minimum magnitude. Results of simulations of electric angular momentum and current quantum beats are presented to demonstrate the time-dependent behaviors of three coherent excited states, $(b_1 + b_2)$ $((b_1 - b_2))$ with A symmetry and $(a + b_1)$ $((a - b_1))$ and $(a + b_2)$ $((a - b_2))$ with B symmetry in the point group C_2. It was found that the value of the bridge bond current depends on the symmetry of the electronic coherence, i.e., the value vanishes for the electronic coherent state $(b_1 + b_2)$ $((b_1 - b_2))$ with A symmetry, while it is nonzero for the two electronic coherence states $(a + b_1)$ $((a - b_1))$ and $(a + b_2)$ $((a - b_2))$ with B symmetry. The initial direction of the coherent ring current for each of the electronic coherence state $(a + b_1)$ $((a - b_1))$ and $(a + b_2)$ $((a - b_2))$ with B symmetry can be determined by evaluating the corresponding bridge bond current density. The direction of the coherent ring current is parallel to the X-axis. The direction of the resultant coherent ring current for the electronic coherent state $(b_1 + b_2)$ $((b_1 - b_2))$ is, on the other hand, parallel to the Z-axis and its direction changes as the period of the quantum beat frequency, and the direction of the current between two electronic coherences, $(b_1 + b_2)$ and $(b_1 - b_2)$, is π phase-shifted. The initial phase can be determined by calculation of the phase of bond currents for each electronic coherence. Furthermore, evaluation of the ring current-induced magnetic field indicates the possibility of a control parameter for a two-dimensional ultrafast switching device as well as the ring current itself when dephasing processes are slow. Manipulation of the magnetic order by ultrashort laser pulses has become a fundamental topic for solid physics and quantum computation.[57] Thus, it should become possible to measure ring current-induced magnetic fields of aromatic molecules in the near future. In the present treatment, rigorous consideration of nonadiabatic coupling effects was omitted, though some effects of electron-nuclear interaction are implicitly taken into account by introducing dephasing constants. An explicit dynamical treatment is necessary to quantitatively describe the whole electronic and nuclear dynamics of a real system.[31,58] In particular, the out-of-plane bending vibration of the two phenol rings is expected to have a significant effect on coherent electronic dynamics.[59] Results of detailed investigation of dephasing effects on coherent ring currents of chiral molecules in condensed phases will be presented elsewhere.

ACKNOWLEDGMENTS

We are grateful to Professor M. Hayashi for his useful comments on the electronic structure theory of molecules. This work was supported by a JSPS Research Grant (No. 23550003) and the National Science Council of Taiwan. H.M. would like to thank Professor J.-L. Kuo for his critical comments and supports.

APPENDIX A: π-ELECTRON ANGULAR MOMENTUM

By using Eq. (6) with the angular momentum operator of the Z-component $\vec{l}_{zK} = -i\hbar(x_K\partial/\partial y_K - y_K\partial/\partial x_K)\vec{n}_K$, we can express an angular momentum created on phenol ring K (L or R) as

$$\int d^3r_K \langle \vec{l}_{zK} \rangle = 2n\hbar\vec{n}_K \sum_{\alpha<\beta} \mathrm{Im}\rho_{\beta\alpha}(t) \sum_{ij\in K} \left(\delta_{ab} c^*_{a'i} c_{b'j} + \delta_{a'b'} c^*_{ai} c_{bj}\right) \times \int d^3r \chi^*_i \left(x\frac{\partial}{\partial y} - y\frac{\partial}{\partial x}\right)\chi_j, \tag{A1}$$

where $\vec{n}_K$ is the direction of the angular momentum that is a unit vector perpendicular to ring K, and χ_i and χ_j are AOs at atomic sites i and j, respectively. We adopt Slater AOs for estimation of the integral $\int d^3r \chi^*_i (x\frac{\partial}{\partial y} - y\frac{\partial}{\partial x})\chi_j$ in Eq. (A1). We use $3p_z$ Slater AOs in addition to $2p_z$ Slater AOs. Atomic orbital χ_i can be expressed as $\chi_i = c_{2p,i}\chi_{2p,i} + c_{3p,i}\chi_{3p,i}$ where $c_{2p,i}$ and $c_{3p,i}$ are the $2p$ and $3p$ components of $2p_z$ and $3p_z$ Slater orbitals, $\chi_{2p,i}$ and $\chi_{3p,i}$, which are given as $\chi_{2p,i} = \chi_{2p}(\vec{r} - \vec{r}_i) = \frac{z}{\sqrt{\pi a_2^5}} \exp(-|\vec{r} - \vec{r}_i|/a_2)$ with $a_2 = \frac{2a_0}{Z_{eff}} = \frac{2.0}{3.25} = 0.6154$ and $\chi_{3p,i} = \chi_{3p}(\vec{r} - \vec{r}_i) = \frac{\sqrt{2}z}{\sqrt{15\pi a_3^5}}(|\vec{r} - \vec{r}_i|/a_3)\exp(-|\vec{r} - \vec{r}_i|/a_3)$ with $a_3 = 1.5a_2 = 0.9231$, respectively. Here, the phenol ring is set on the xy-plane.

By defining $l_{ij}(n, n') \equiv \int d^3r \chi^*_{np,i}(x\frac{\partial}{\partial y} - y\frac{\partial}{\partial x})\chi_{n'p,j}$, we obtain $\int d^3r \chi^*_i(x\frac{\partial}{\partial y} - y\frac{\partial}{\partial x})\chi_j$ as

$$\int d^3r \chi^*_i \left(x\frac{\partial}{\partial y} - y\frac{\partial}{\partial x}\right)\chi_j = c^*_{2p,i}c_{2p,j}l_{ij}(2,2) + c^*_{2p,i}c_{3p,j}l_{ij}(2,3) + c^*_{3p,i}c_{2p,j}l_{ij}(3,2) + c^*_{3p,i}c_{3p,j}l_{ij}(3,3). \tag{A2}$$

By shifting the coordinates $\vec{r}' = \vec{r} - \frac{\vec{r}_i + \vec{r}_j}{2}$, we can express $l_{ij}(n, n')$ in Eq. (A2) as

$$l_{ij}(n,n') \equiv \int d^3r \chi^*_{np,i}\left(x\frac{\partial}{\partial y} - y\frac{\partial}{\partial x}\right)\chi_{n'p,j} = \int d^3r' \chi_n\left(\vec{r}' - \frac{\vec{r}_i - \vec{r}_j}{2}\right) \times \left(x\frac{\partial}{\partial y} - y\frac{\partial}{\partial x}\right)_{\vec{r}=\vec{r}'+(\vec{r}_i+\vec{r}_j)/2} \chi_{n'}\left(\vec{r}' + \frac{\vec{r}_i - \vec{r}_j}{2}\right). \tag{A3}$$

Let us now introduce new coordinates (X, Y, Z) that are obtained by rotating the coordinates (x, y, z) around $\vec{r}' = \vec{0}$ by angle ϕ so that $\vec{r}_i - \vec{r}_j$ becomes parallel to the X-axis as is shown in Fig. 9,

$$\cos\phi = \frac{\vec{e}_x \cdot (\vec{r}'_i - \vec{r}'_j)}{r_{ij}} = \frac{x_i - x_j}{r_{ij}}, \tag{A4a}$$

$$\sin\phi = \frac{y_i - y_j}{r_{ij}}, \tag{A4b}$$

where $\vec{e}_x$ is a unit vector along the x-axis and $r_{ij} = |\vec{r}_i - \vec{r}_j|$. Then, the coordinates $\vec{R} = (X, Y, Z)$ after ϕ rotation are

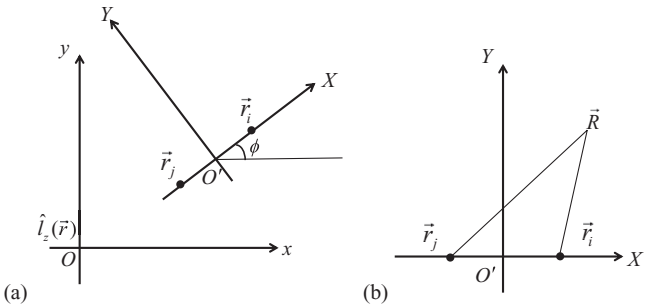

FIG. 9. (a) Relation between the molecular frame denoted by xy and that of the new frame XY for evaluation of angular momentum at O, the direction of which is perpendicular to the molecular plane, xOy. $\hat{l}_z(\vec{r})$ is the angular momentum operator. (b) Coordinates $\vec{R}(X, Y)$ on the new frame.

defined as shown in Fig. 9 as

$$\vec{r}' = R(\phi)\vec{R} = \begin{pmatrix} \cos\phi & -\sin\phi & 0 \\ \sin\phi & \cos\phi & 0 \\ 0 & 0 & 1 \end{pmatrix} \begin{pmatrix} X \\ Y \\ Z \end{pmatrix}. \quad \text{(A5)}$$

Thus, the integral in Eq. (A3) can be expressed as

$$\begin{aligned} &\int d^3r\, \chi^*_{np,i} \left(x\frac{\partial}{\partial y} - y\frac{\partial}{\partial x} \right) \chi_{n'p,j} \\ &= \int d^3R\, \chi^*_n \left(R(\phi) \left(\vec{R} - R(-\phi)\frac{\vec{r}_i - \vec{r}_j}{2} \right) \right) \\ &\times \left[\left(X\cos\phi - Y\sin\phi + \frac{x_i + x_j}{2} \right) \right. \\ &\times \left(\sin\phi\frac{\partial}{\partial X} + \cos\phi\frac{\partial}{\partial Y} \right) \\ &- \left(X\sin\phi + Y\cos\phi + \frac{y_i + y_j}{2} \right) \\ &\left. \times \left(\cos\phi\frac{\partial}{\partial X} - \sin\phi\frac{\partial}{\partial Y} \right) \right] \\ &\times \chi_{n'} \left(R(\phi) \left(\vec{R} + R(-\phi)\frac{\vec{r}_i - \vec{r}_j}{2} \right) \right) \\ &= \int d^3R\, \chi^*_n(\vec{R} - \vec{R}_{ij}/2) \left(X\frac{\partial}{\partial Y} - Y\frac{\partial}{\partial X} \right. \\ &\left. + \frac{x_i^2 - x_j^2 + y_i^2 - y_j^2}{2r_{ij}}\frac{\partial}{\partial Y} + \frac{x_j y_i - x_i y_j}{r_{ij}}\frac{\partial}{\partial X} \right) \\ &\times \chi_{n'}(\vec{R} + \vec{R}_{ij}/2) \end{aligned} \quad \text{(A6)}$$

with $\vec{R}_{ij} = (r_{ij}, 0, 0)$.

Because the terms linear to Y vanish, Eq. (A6) becomes

$$\begin{aligned} &\int d^3r\, \chi^*_{n,i} \left(x\frac{\partial}{\partial y} - y\frac{\partial}{\partial x} \right) \chi_{n',j} \\ &= \frac{x_j y_i - x_i y_j}{r_{ij}} \int d^3R\, \chi^*_{np,i}(\vec{R} - \vec{R}_{ij}/2) \\ &\times \frac{\partial}{\partial X}\chi_{n'p,j}(\vec{R} + \vec{R}_{ij}/2). \end{aligned} \quad \text{(A7)}$$

Using the elliptic coordinates $\xi = (R_i + R_j)/r_{ij}$ and $\eta = (R_i - R_j)/r_{ij}$, where $R_i = |\vec{R} - \vec{R}_{ij}/2| = \frac{r_{ij}}{2}(\xi + \eta)$, $R_j = |\vec{R} + \vec{R}_{ij}/2| = \frac{r_{ij}}{2}(\xi - \eta)$, and $X = -\frac{r_{ij}}{2}\xi\eta$, we finally obtain

$$\begin{aligned} l_{ij}(2,2) = &-\frac{x_i y_j - x_j y_i}{15a_2^2} \left(3 + 3\left(\frac{r_{ij}}{a_2}\right) + \left(\frac{r_{ij}}{a_2}\right)^2 \right) \\ &\times \exp(-r_{ij}/a_2), \end{aligned} \quad \text{(A8a)}$$

$$\begin{aligned} l_{ij}(2,3) = &\frac{x_i y_j - x_j y_i}{15\sqrt{15}(a_2a_3)^{5/2}(a_2 + a_3)^5} 2\sqrt{2}a_2^2 \\ &\times \exp\left(-r_{ij}\left(\frac{1}{a_2} + \frac{1}{a_3} \right) \right) \left[24a_2^2a_3^3(-4a_2 + 3a_3) \right. \\ &- 12a_2(4a_2 - a_3)a_3^2(a_2 + a_3)r_{ij} - 2(5a_2 - a_3) \\ &\left. \times a_3(a_2 + a_3)^2 r_{ij}^2 - (a_2 + a_3)^3 r_{ij}^3 \right], \end{aligned} \quad \text{(A8b)}$$

$$\begin{aligned} l_{ij}(3,2) = &-\frac{x_i y_j - x_j y_i}{15\sqrt{15}(a_2a_3)^{3/2}(a_2 + a_3)^5} 2\sqrt{2} \\ &\times \exp\left(-\frac{r_{ij}}{2}\left(\frac{1}{a_2} + \frac{1}{a_3} \right) \right) \\ &\times \left(72a_2^3a_3^3 + 36a_2^2a_3^2(a_2 + a_3)r_{ij} \right. \\ &\left. + 8a_2a_3(a_2 + a_3)^2 r_{ij}^2 + (a_2 + a_3)^3 r_{ij}^3 \right), \end{aligned} \quad \text{(A8c)}$$

and

$$\begin{aligned} l_{ij}(3,3) = &-\frac{x_i y_j - x_j y_i}{1575a_3^2} \left(147 + 147\left(\frac{r_{ij}}{a_3}\right) + 65\left(\frac{r_{ij}}{a_3}\right)^2 \right. \\ &\left. + 16\left(\frac{r_{ij}}{a_3}\right)^3 + 3\left(\frac{r_{ij}}{a_3}\right)^4 \right) \exp(-r_{ij}/a_3). \end{aligned} \quad \text{(A8d)}$$

APPENDIX B: EVALUATION OF J_{ij}^{IABC}

For evaluation of bond currents of a nonplanar molecule with two aromatic rings combined with a single bond, we have to take into account two types of bond current, that of each aromatic ring and that of the bridge bond. To derive an expression for both currents, we express $2p$- and $3p$-orbitals in terms of a vector perpendicular to aromatic ring K as

$$\chi_{2p,i} = \frac{\vec{n}_{K_i} \cdot (\vec{r} - \vec{r}_i)}{\sqrt{\pi a_2^5}} \exp(-|\vec{r} - \vec{r}_i|/a_2) \quad \text{(B1a)}$$

and

$$\chi_{3p,i} = \frac{\sqrt{2}\vec{n}_{K_i} \cdot (\vec{r} - \vec{r}_i)}{\sqrt{15\pi a_3^5}} (|\vec{r} - \vec{r}_i|/a_3) \exp(-|\vec{r} - \vec{r}_i|/a_3), \quad \text{(B1b)}$$

where K_i denotes the phenol ring that the carbon atom i belongs to.

In the case in which the half-plane S is at the center of bond C_i–C_j, the IABC as shown in Fig. 10,

$$J_{ij}^{\text{IABC}} = \frac{1}{2}\int_S d^2r_\perp \vec{n}_\perp \cdot \chi_i^*(\vec{\nabla} - \overleftarrow{\nabla})\chi_j, \quad \text{(B2)}$$

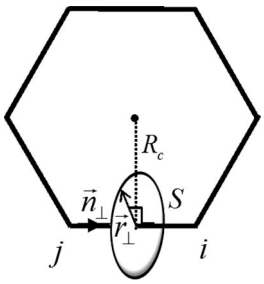

FIG. 10. Coordinates for the inter-atomic bond current from atom j to the nearest neighbor atom i, $J_{ij}^{\mathrm{IABC}(S\text{ at center})} = \int_S d^2r_\perp \chi_i^* \vec{n}_\perp \cdot \vec{\nabla}\chi_j$ in a hexagonal ring, which determines the current passing through a half-plane S perpendicular to the bond at the center R_c.

becomes

$$J_{ij}^{\mathrm{IABC}} = \int_S d^2r_\perp \vec{n}_\perp \cdot \chi_i^* \vec{\nabla}\chi_j \equiv J_{ij}^{\mathrm{IABC}(S\text{ at center})}. \quad \text{(B3)}$$

Equation (B3) can be expressed as

$$J_{ij}^{\mathrm{IABC}} = c_{2p,i}^* c_{2p,j} J_{ij}(2,2) + c_{2p,i}^* c_{3p,j} J_{ij}(2,3) + c_{3p,i}^* c_{2p,j} J_{ij}(3,2) + c_{3p,i}^* c_{3p,j} J_{ij}(3,3) \quad \text{(B4)}$$

with $J_{ij}(n,n') \equiv \int_S d^2r_\perp \chi_{np,i}^* \vec{n}_\perp \cdot \vec{\nabla}\chi_{n'p,j}$.

When we define the integral variables s, u, a unit vector $\vec{r}_{\perp,l} = \vec{n}_\perp \times \vec{n}_{K_l}$ for $l = i, j$, and set a half-plane S at the middle of the chemical bond i and j (see Fig. 10), $\vec{r}$ becomes $\vec{r} = \frac{\vec{r}_i + \vec{r}_j}{2} + s\vec{n}_{K_i} + u\vec{r}_{\perp,i}$, where $\vec{n}_{K_i} \cdot \vec{n}_\perp = \vec{r}_{\perp,i} \cdot \vec{n}_\perp = \vec{n}_{K_i} \cdot \vec{r}_{\perp,i} = 0$.

By using the relations

$$\int_S d^2r_\perp \chi_{np,i}^* \vec{n}_\perp \cdot \vec{\nabla}\chi_{2p,j} = \frac{-1}{a_2} \int_S d^2r_\perp \chi_{np,i}^* \chi_{2p,j} \frac{\vec{n}_\perp \cdot (\vec{r} - \vec{r}_j)}{|\vec{r} - \vec{r}_j|} \quad \text{(B5a)}$$

and

$$\int_S d^2r_\perp \chi_{np,i}^* \vec{n}_\perp \cdot \vec{\nabla}\chi_{3p,j} = \int_S d^2r_\perp \chi_{np,i}^* \chi_{3p,j} \frac{\vec{n}_\perp \cdot (\vec{r} - \vec{r}_j)}{|\vec{r} - \vec{r}_j|} \times \left(\frac{1}{|\vec{r} - \vec{r}_j|} - \frac{1}{a_3} \right), \quad \text{(B5b)}$$

$J_{ij}(2,2)$ in Eq. (B4) becomes

$$J_{ij}(2,2) = -\int_S ds du \frac{s(s\vec{n}_{K_i} \cdot \vec{n}_{K_j} + u\vec{n}_{K_i} \cdot \vec{r}_{\perp,j})}{2\pi a_2^6 \sqrt{r_{ij}^2/4 + s^2 + u^2}} r_{ij} \times \exp\left(-2\sqrt{r_{ij}^2/4 + s^2 + u^2}/a_2 \right). \quad \text{(B6)}$$

By transforming the variables $s = r\cos\theta$ and $u = r\sin\theta$ we have

$$J_{ij}(2,2) = \cos\theta_d \frac{r_{ij}}{2a_2^6} \int_0^\infty dr \frac{r^3 \exp\left(-2\sqrt{r_{ij}^2/4 + r^2}/a_2 \right)}{\sqrt{r_{ij}^2/4 + r^2}}, \quad \text{(B7a)}$$

where θ_d is the dihedral angle between two phenols. For two planar phenols, $\theta_d = \pi$. Similarly, we obtain

$$J_{ij}(2,3) = -\frac{r_{ij}\cos\theta_d}{\sqrt{30a_2^5a_3^7}} \int_0^\infty dr \frac{r^3}{\sqrt{r_{ij}^2/4 + r^2}} \times \left(1 - \frac{\sqrt{r_{ij}^2/4 + r^2}}{a_3} \right) \times \exp\left(-\sqrt{r_{ij}^2/4 + r^2}\left(a_2^{-1} + a_3^{-1}\right) \right), \quad \text{(B7b)}$$

$$J_{ij}(3,2) = \frac{r_{ij}\cos\theta_d}{\sqrt{30a_2^7a_3^7}} \int_0^\infty dr r^3 \times \exp\left(-\sqrt{r_{ij}^2/4 + r^2}\left(a_2^{-1} + a_3^{-1}\right) \right), \quad \text{(B7c)}$$

and

$$J_{ij}(3,3) = \frac{-r_{ij}\cos\theta_d}{15a_3^7} \int_0^\infty dr r^3 \left(1 - \frac{\sqrt{r_{ij}^2/4 + r^2}}{a_3} \right) \times \exp\left(-2a_3^{-1}\sqrt{r_{ij}^2/4 + r^2} \right). \quad \text{(B7d)}$$

Consider now the inter-atomic bond current in an extreme case in which the current that is perpendicular to a half-plane S (x = 0) at site C_j of bond C_i–C_j as shown in Fig. 11. Here, if we use $2p_z$ Slater AOs, the integral

$$J_{ij}^{\mathrm{IABC}} = \frac{1}{2} \int_S d^2r_\perp \vec{n}_\perp \cdot \chi_{2p,i}^* (\vec{\nabla} - \overleftarrow{\nabla}) \chi_{2p,j} \left(\equiv J_{ij}^{\mathrm{IABC}(S\text{ at site})} \right) \quad \text{(B8)}$$

can be expressed by using $\int_S d^2r_\perp \vec{n}_\perp \cdot \chi_{2p,i}^* \vec{\nabla}\chi_{2p,j} = 0$, as

$$\begin{aligned} J_{ij}^{\mathrm{IABC(S\text{ at site})}} &= -\frac{1}{2} \int_S d^2r_\perp \vec{n}_\perp \cdot \chi_{2p,j} \nabla \chi_{2p,i}^* \\ &= -\frac{1}{2} \int dydz \chi_{2p}(\vec{r}) \vec{n}_\perp \cdot \left(-\vec{n}_K \cdot (\vec{r} - \vec{r}_i) \frac{\vec{r} - \vec{r}_i}{a_2 |\vec{r} - \vec{r}_i|} \right) \times \frac{\exp(-|\vec{r} - \vec{r}_i|/a_2)}{\sqrt{\pi a_2^5}} \Bigg|_{x=0} \\ &= \frac{1}{2} \int dydz \chi_{2p}(\vec{r}) z \left(\frac{x - \sqrt{3}r_{ij}/2}{a_2 |\vec{r} - \vec{r}_i|} \right) \times \frac{\exp(-|\vec{r} - \vec{r}_i|/a_2)}{\sqrt{\pi a_2^5}} \Bigg|_{x=0}, \end{aligned} \quad \text{(B9)}$$

where $|\vec{r} - \vec{r}_i|_{x=0} = \sqrt{(y - r_{ij}/2)^2 + z^2 + 3r_{ij}^2/4}$.

The magnitude of the inter-atomic bond current calculated on the half plane at the carbon site can be expressed in terms of that calculated on the half plane at the center of the

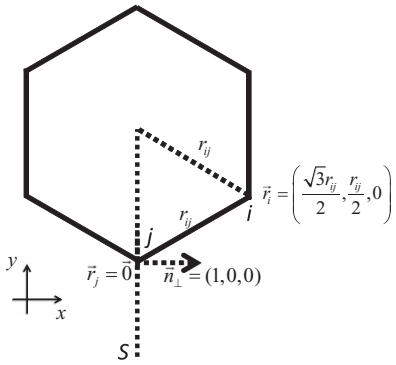

FIG. 11. Coordinates for the inter-atomic bond current, $J_{ij}^{\mathrm{IABC}(S \text{ at site})}$, which is perpendicular to a half-plane S (x = 0) at carbon nuclei C_j of bond C_i–C_j.

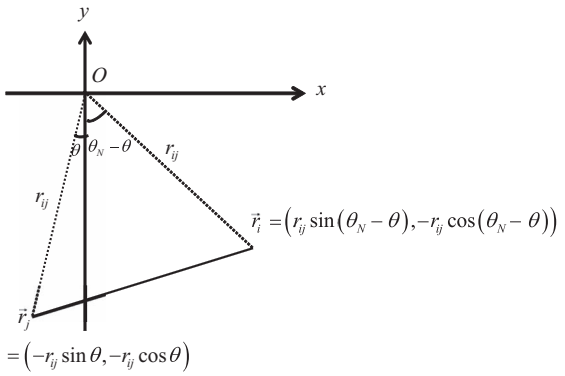

FIG. 12. Coordinates for the inter-atomic bond current in a general case. The half plane S is set at a position between carbon atomic sites, C_i and C_j. N is the number of carbon atoms. Angle θ is defined in the range $0 \le \theta \le \theta_N$ in which θ_N is the angle between C_i and C_j from the center of the ring.

bond as

$$J_{ij}^{\mathrm{IABC}(S \text{ at site})} = 0.32 J_{ij}^{\mathrm{IABC}(S \text{ at center})}, \tag{B10}$$

where $r_{ij} = 0.14$ nm and $a_2 = 2.0/3.25 = 0.615$ were used.

We now consider a general case in which half-plane S is set at a position between two atomic sites C_i and C_j as shown in Fig. 12. Here, the ring consists of six carbon atoms ($N = 6$). The expression for the current is derived using $2p_z$ Slater AOs as

$$\begin{aligned} J_{ij}^{\mathrm{IABC}}(\theta) &= \frac{1}{2}\int_S d^2 r_\perp \vec{n}_\perp \cdot \chi_i^*(\vec{\nabla} - \overleftarrow{\nabla})\chi_j \\ &= \frac{1}{2}\int dydz \Bigg[\chi_{2p}(\vec{r} - \vec{r}_i)\vec{n}_x \\ &\quad \cdot \left(\vec{n}_z - \vec{n}_z \cdot (\vec{r} - \vec{r}_j)\frac{\vec{r} - \vec{r}_j}{a_2|\vec{r} - \vec{r}_j|}\right) \\ &\quad \times \frac{\exp(-|\vec{r} - \vec{r}_j|/a_2)}{\sqrt{\pi a_2^5}}\Bigg|_{x=0} - \chi_{2p}(\vec{r} - \vec{r}_j)\vec{n}_x \\ &\quad \cdot \left(\vec{n}_z - \vec{n}_z \cdot (\vec{r} - \vec{r}_i)\frac{\vec{r} - \vec{r}_i}{a_2|\vec{r} - \vec{r}_i|}\right) \\ &\quad \times \frac{\exp(-|\vec{r} - \vec{r}_i|/a_2)}{\sqrt{\pi a_2^5}}\Bigg|_{x=0}\Bigg] \\ &= \frac{1}{2\pi a_2^6}\int dydz\, z^2 \exp(-|\vec{r} - \vec{r}_i|/a_2 \\ &\quad - |\vec{r} - \vec{r}_j|/a_2)_{x=0}\left(\frac{x_i}{|\vec{r} - \vec{r}_i|} - \frac{x_j}{|\vec{r} - \vec{r}_j|}\right), \end{aligned} \tag{B11}$$

where $|\vec{r} - \vec{r}_{i,j}| = \sqrt{x_{i,j}^2 + z^2 + (y - y_{i,j})^2}$, $x_j = -r_{ij}\sin\theta$, $y_j = -r_{ij}\cos\theta$, $x_i = r_{ij}\sin(\theta_N - \theta)$, and $y_i = -r_{ij}\cos(\theta_N - \theta)$ with $0 \le \theta \le \theta_N = \frac{2\pi}{N}$.

The average of the current for a hexagonal ring is given by

$$\frac{1}{\theta_N}\int_0^{\theta_N} d\theta\, J_{ij}^{\mathrm{IABC}}(\theta) = 0.742 J_{ij}^{\mathrm{IABC}}(\pi/6). \tag{B12}$$

APPENDIX C: SELECTIVE GENERATION OF A TWO-ELECTRONIC COHERENT STATE IN A THREE-ELECTRONIC STATE (DERIVATION OF EQ. (15b))

The polarization vector $\vec{e}^{\pm}$ is given in terms of arbitrary linear independent basis vectors for convenience of calculation. Here, choose orthogonal basis vectors like

$$\vec{e}_{ab2}^{\pm} = c_a^{\pm}\vec{\mu}_{gb1} \times \vec{\mu}_{gb2} + c_{b1}^{\pm}\vec{\mu}_{gb2} \times \vec{\mu}_{ga} + c_{b2}^{\pm}\vec{\mu}_{ga} \times \vec{\mu}_{gb1}. \tag{C1}$$

Due to the fact that this polarization vector should satisfy Eq. (15a), we obtain $c_{b1}^{\pm} = 0$ and $(c_a^{\pm} \mp c_{b2}^{\pm})\vec{\mu}_{ga} \cdot (\vec{\mu}_{gb1} \times \vec{\mu}_{gb2}) = 0$. Since $\vec{\mu}_{ga} \cdot (\vec{\mu}_{gb1} \times \vec{\mu}_{gb2}) \neq 0$, $c_a^{\pm} = \pm c_{b2}^{\pm}$, and normalization of the polarization vector $|\vec{e}_{ab2}^{\pm}| = 1$, $\vec{e}_{ab2}^{\pm}$ yields

$$\vec{e}_{ab2}^{\pm} = \frac{(\vec{\mu}_{ga} \mp \vec{\mu}_{gb2}) \times \vec{\mu}_{gb1}}{|(\vec{\mu}_{ga} \mp \vec{\mu}_{gb2}) \times \vec{\mu}_{gb1}|}. \tag{C2}$$

APPENDIX D: MAGNETIC FIELD INDUCED BY A CURRENT DENSITY

We derive an expression for the magnetic field at time t at z above the center of the ring K, $B_K(t, z)$, induced by a distribution of the π-electron ring current density around the aromatic ring. The induced magnetic field at height h is created by the ring current density, $J_K(t)f(x, z)dxdz$, as is depicted in Fig. 13. Then the induced magnetic field at height h toward the z-axis is given by

$$B_K(t, h) = \int \frac{\mu_0}{2R}\langle J(t)\rangle_K f(x, z)\sin^3\theta\, dxdz \tag{D1}$$

with $R_c = \frac{\sqrt{3}}{2}r_{ij}$.

$f(x, z)$ is proportional to

$$f(x, z) \propto \vec{n}_\perp \cdot \chi_i^*\vec{\nabla}\chi_j = \frac{z^2 \exp\left(-\frac{2}{a_2}\sqrt{y^2 + z^2 + r_{ij}^2/4}\right)}{2\pi a_2^6\sqrt{y^2 + z^2 + r_{ij}^2/4}}, \tag{D2}$$

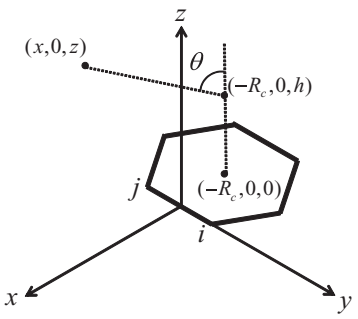

FIG. 13. Coordinates for the induced magnetic field created at the center of ring K at height h by a ring current density $\langle J(t)\rangle_K f(x, z)dxdz$. The bond between i and j lies on the y-axis.

which satisfies the normalization condition $\int dxdzf(x, z) = 1$. Angle θ in Eq. (D1) is given by

$$\sin\theta = \frac{|x + \sqrt{3}r_{ij}/2|}{\sqrt{(x + \sqrt{3}r_{ij}/2)^2 + (z - h)^2}}. \tag{D3}$$

Under the limit of $h \to \infty$, by using $\sin\theta \to \frac{|x+\sqrt{3}r_{ij}/2|}{h}$, $B_K(t, h)$ becomes

$$B_K(t, h) \to \int \frac{\mu_0}{2R_c}\langle J(t)\rangle_K f(x, z)\frac{|x + \sqrt{3}r_{ij}/2|^3}{h^3}dxdz, \tag{D4}$$

whereas $B_K^{\mathrm{SRL}}(t, h)$ becomes

$$B_K^{\mathrm{SRL}}(t, h) \to \frac{\mu_0\langle J(t)\rangle_K}{2r_{ij}}\left(\frac{r_{ij}}{h}\right)^3, \tag{D5}$$

where we use $\sin\eta \to \frac{r_{ij}}{h}$. Thus, $B_K(t, h \to \infty) = 0.88B_K^{\mathrm{SRL}}(t, h \to \infty)$.

[1]E. Goulielmakis, Z.-H. Loh, A. Wirth, R. Santra, N. Rohringer, V. S. Yakovlev, S. Zherebtsov, T. Pfeifer, A. M. Azzeer, M. F. Kling, S. R. Leone, and F. Krausz, Nature (London) **466**, 739 (2010).
[2]K.-J. Yuan and A. D. Bandrauk, J. Phys. B **45**, 074001 (2012).
[3]S. Chen, S. Gilbertson, H. Wang, M. Chini, K. Zhao, S. D. Khan, Y. Wu, and Z. Chang, *Advances in Multiphoton Processes and Spectroscopy* (World Scientific, Singapore, 2011), Vol. 20, p. 127.
[4]F. Remacle and R. D. Levine, Phys. Rev. A **83**, 013411 (2011).
[5]P. Tzallas, E. Skantzakis, J. E. Kruse, and D. Charalambidis, *Progress in Ultrafast Intense Laser Science* (Springer, Heidelberg, 2011), Vol. 7, p. 163.
[6]I. S. Ulusoy and M. Nest, J. Am. Chem. Soc. **133**, 20230 (2011).
[7]Y. Fujimura and H. Sakai, *Electronic and Nuclear Dynamics in Molecular Systems* (World Scientific, Singapore, 2011), p. 117.
[8]K. P. Singh, F. He, P. Ranitovic, W. Cao, S. De, D. Ray, S. Chen, U. Thumm, A. Becker, M. M. Murnane, H. C. Kapteyn, I. V. Litvinyuk, and C. L. Cocke, Phys. Rev. Lett. **104**, 023001 (2010).
[9]F. Krausz and M. Ivanov, Rev. Mod. Phys. **81**, 163 (2009).
[10]M. Nest, F. Remacle, and R. D. Levine, New J. Phys. **10**, 025019 (2008).
[11]M. F. Kling and M. J. J. Vrakking, Annu. Rev. Phys. Chem. **59**, 463 (2008).
[12]S. S. Skourtis, D. N. Bernata, R. Naaman, A. Nitzan, and D. H. Waldeck, Phys. Rev. Lett. **101**, 238103 (2008).
[13]Y. Nabekawa and K. Midorikawa, *Advances in Multiphoton Processes and Spectroscopy* (World Scientific, Singapore, 2008), Vol. 18, p. 1.
[14]M. Lein and C. C. Chirilă, *Advances in Multiphoton Processes and Spectroscopy* (World Scientific Singapore, 2008), Vol. 18, p. 69.
[15]P. B. Corkum and F. Krausz, Nat. Phys. **3**, 381 (2007).
[16]F. Remacle, M. Nest, and R. D. Levine, Phys. Rev. Lett. **99**, 183902 (2007).
[17]E. Räsänen, A. Castro, J. Werchnik, A. Rubio, and E. K. U. Gross, Phys. Rev. Lett. **98**, 157404 (2007).
[18]T. Klamroth, J. Chem. Phys. **124**, 144310 (2006).
[19]P. Krause, T. Klamroth, and P. Saalfrank, J. Chem. Phys. **123**, 074105 (2005).
[20]Y. V. Pershin and C. Piermarocchi, Phys. Rev. B **72**, 245331 (2005).
[21]H. Niikura, F. Légaré, R. Hasbani, M. Y. Ivanov, D. M. Villeneuve, and P. B. Corkum, Nature (London) **421**, 826 (2003).
[22]K. Haruyama, H. Kono, Y. Fujimura, I. Kawata, and A. D. Bandrauk, Phys. Rev. A **66**, 043403 (2002).
[23]J. E. Anthony, Chem. Rev. **106**, 5028 (2006).
[24]A. D. Bonifas and R. L. McGreery, Nat. Nanotechnol. **5**, 612 (2010).
[25]I. Barth and J. Manz, Angew. Chem., Int. Ed. **45**, 2962 (2006).
[26]I. Barth, J. Manz, Y. Shigeta, and K. Yagi, J. Am. Chem. Soc. **128**, 7043 (2006).
[27]I. Barth and J. Manz, *Progress in Ultrafast Intense Laser Science* (Springer, 2010), Vol. VI, p. 21.
[28]K. Nobusada and K. Yabana, Phys. Rev. A **75**, 032518 (2007).
[29]M. Kanno, H. Kono, and Y. Fujimura, Angew. Chem., Int. Ed. **45**, 7995 (2006).
[30]M. Kanno, K. Hoki, H. Kono, and Y. Fujimura, J. Chem. Phys. **127**, 204314 (2007).
[31]M. Kanno, H. Kono, Y. Fujimura, and S. H. Lin, Phys. Rev. Lett. **104**, 108302 (2010).
[32]M. Kanno, H. Kono, and Y. Fujimura, *Progress in Ultrafast Intense Laser Science* (Springer, 2011), Vol. VII, p. 53.
[33]H. Mineo, M. Yamaki, Y. Teranish, M. Hayashi, S. H. Lin, and Y. Fujimura, J. Am. Chem. Soc. **134**, 14279 (2012).
[34]E. Steiner and P. W. Fowler, J. Phys. Chem. A **105**, 9553 (2001).
[35]P. Lazzerretti, Prog. Nucl. Magn. Reson. Spectrosc. **36**, 1 (2000).
[36]A. G. Redfield, Adv. Magn. Reson. **1**, 1 (1965).
[37]G. Lindblad, Commun. Math. Phys. **48**, 119 (1976).
[38]S. H. Lin, C. H. Chang, K. K. Liang, R. Chang, Y. J. Shiu, J. M. Zhang, T. S. Yang, M. Hayashi, and F. C. Hsu, Adv. Chem. Phys. **121**, 1 (2002).
[39]Y. Fujimura, H. Kono, T. Nakajima, and S. H. Lin, J. Chem. Phys. **75**, 99 (1981).
[40]S. H. Lin, J. Chem. Phys. **44**, 3759 (1966).
[41]M. Bixon and J. Jortner, J. Chem. Phys. **48**, 715 (1968).
[42]J. Jortner, Philos. Trans. R. Soc. London, Ser. A **356**, 477 (1998).
[43]V. L. Ermolaev, Russ. Chem. Rev. **70**, 471 (2001).
[44]H. Mineo, M. Kanno, H. Kono, S. D. Cao, S. H. Lin, and Y. Fujimura, Chem. Phys. **392**, 136 (2012).
[45]Y. Suzuki, T. Fuji, T. Horio, and T. Suzuki, J. Chem. Phys. **132**, 174302 (2010).
[46]K. Oda, M. Hita, S. Minemoto, and H. Sakai, Phys. Rev. Lett. **104**, 213901 (2010).
[47]M. J. Frisch, G. W. Trucks, H. B. Schlegel *et al.*, GAUSSIAN 09, Revision E.01, Gaussian, Inc., Wallingford, CT, 2009.
[48]D. Jacquemin, V. Wathelet, E. A. Perpète, and C. Adamo, J. Chem. Theory Comput. **5**, 2420 (2009).
[49]See for example, J. S. Baskin, P. M. Felker, and A. H. Zewail, J. Chem. Phys. **84**, 4708 (1986).
[50]Y. Acremann, M. Buess, C. H. Back, M. Dumm, G. Bayreuther, and D. Pescia, Nature (London) **414**, 51 (2001).
[51]V. V. Kruglyak, M. E. Portnoi, and R. J. Hicken, J. Nanophotonics **1**, 013502 (2007).
[52]A. Kirilyuk, A. V. Kimel, and T. Rasing, Rev. Mod. Phys. **82**, 2731 (2010).
[53]I. Barth and J. Manz, Phys. Rev. A **75**, 012510 (2007).

[54]I. Barth, J. Manz, and L. Serrano-Andrés, Chem. Phys. **347**, 263 (2008).
[55]I. Barth, L. Serrano-Andrés, and T. Seideman, J. Chem. Phys. **129**, 164303 (2008).
[56]M. Kanno, Y. Ono, H. Kono, and Y. Fujimura, J. Phys. Chem. A **116**, 11260 (2012).
[57]M. A. Nielsen and I. I. Chuang, *Quantum Computation and Quantum Information*, 10th Anniversary ed. (Cambridge University Press, 2010), p. 13.
[58]K. Moore and H. Rabitz, Nat. Chem. **4**, 72 (2012).
[59]S. M. Parker, M. A. Ratner, and T. Seideman, J. Chem. Phys. **135**, 224301 (2011).